New Family of Explicit Structure-Dependent Integration Algorithms with Controllable Numerical Dispersion

Yu Tang, Ph.D., M.ASCE[1]; Dawei Ren[2]; Hui Qin, Ph.D.[3]; and Chao Luo, Ph.D.[4]

Abstract: Direct integration algorithms are effective methods to solve the temporally discretized differential equations of motion for structural dynamics. Numerous researchers have worked out various algorithms to achieve desirable properties of explicit expression, unconditional stability, and controllable numerical dissipation. However, studies involving the numerical dispersion of integration algorithms are limited. In this paper, a precorrected bilinear transformation from a continuous domain to a discrete domain associating with pole-matching based on the control theory is utilized to develop a new family of explicit structure-dependent integration algorithms, referred to as TL-φ algorithms. In contrast to the existing algorithms, the significant improvement of the proposed method is that it can control the amount of numerical dispersion by an additional parameter related to the critical frequency of the structure. Stability, energy dissipation, and numerical dispersion properties of the proposed algorithms for both linear and nonlinear systems are fully studied. It is shown that the proposed family of algorithms is unconditionally stable for linear systems while only conditionally stable for nonlinear systems. Though the numerical dissipation property of the TL-φ algorithms is quite similar to that of other well-developed methods, its ability to minimize the period errors when compared with other methods makes it beneficial to the accuracy of the numerical simulation of dynamic responses. Four numerical examples are used to investigate the improved performance of the new method, and the results show that the proposed algorithms can be potentially used to solve linear and nonlinear structural dynamic problems with desirable numerical dispersion performance. **DOI: 10.1061/(ASCE)EM.1943-7889.0001901.** © *2021 American Society of Civil Engineers.*

Author keywords: Explicit integration algorithm; Structure-dependent; Unconditionally stable; Controllable numerical dispersion; Linear and nonlinear structural dynamics.

Introduction

In numerical simulations, direct integration algorithms are used to solve the temporally discretized equations of motion (EOMs) to study the response of a structure subjected to seismic/dynamic excitation (Butcher 2003; Bonnetr et al. 2008; Darby et al. 2001). Numerous integration algorithms (Newmark 1959; Hilber et al. 1977; Chung and Lee 1994; Chang 2014; Feng et al. 2018; Guo et al. 2018; Kolay and Ricles 2019; Li and Yu 2019) have been developed in the past. In general, all the existing algorithms can be classified into two categories, i.e., explicit and implicit. An integration algorithm is said to be explicit if the displacement and velocity at the current time step can be expressed in terms of all the known responses at the previous time steps (Shing and Mahin 1985), such as the central difference method (Yu and Zou 2016) and the Newmark explicit scheme (Zhai 1996); otherwise the algorithm is implicit, such as the Newmark implicit algorithms (Newmark 1959), the Wilson-θ method (Wilson et al. 1973), and the HHT-α method (Hilber et al. 1977). Explicit algorithms are preferred over implicit ones because they involve no nonlinear iterations during a step-by-step simulation and show a higher calculation efficiency for long-time simulations with small time steps. However, explicit algorithms are usually conditionally stable, which leads to a time-step size restriction imposed by the stability requirement, especially for a multi-degree-of-freedom (MDOF) system with high natural frequencies. Thus, integration algorithms that possess both explicit expression and unconditional stability are worthy of attention.

In recent years, a new type of integration algorithm called structure-dependent algorithms has been published for solving dynamic problems. In contrast to the traditional algorithms that have structure-independent integration parameters in the expressions of displacement and velocity, the integration parameters in a structure-dependent algorithm are determined by the initial structural properties, including natural frequency and damping ratio of the system and time steps (Chang et al. 2017). The first structure-dependent integration algorithm was proposed by Chang (2002) for pseudodynamic testing (named the Chang explicit method), in which the displacement increment is explicit in form while that for the velocity is implicit. This algorithm is deemed to be second-order accurate and unconditionally stable for linear and instantaneous stiffness softening systems (Chang and Liao 2005). Chen and Ricles (2008a) proposed another type of structure-dependent integration algorithm (namely, the CR algorithm) based on discrete control theory, in which both the displacement and velocity increments are explicit in form. The CR algorithm has been successfully implemented in many real-time hybrid simulation (RTHS), and it is noted that this method is unconditionally stable for linear and instantaneous stiffness softening systems and possesses second-order accuracy as well (Chen et al. 2008). Then, some researchers worked

[1]School of Hydraulic Engineering, Dalian Univ. of Technology, Dalian, Liaoning 116024, China. ORCID: https://orcid.org/0000-0002-7604-155X

[2]School of Hydraulic Engineering, Dalian Univ. of Technology, Dalian, Liaoning 116024, China.

[3]State Key Laboratory of Coastal and Offshore Engineering, Dalian Univ. of Technology, Dalian, Liaoning 116024, China (corresponding author). ORCID: https://orcid.org/0000-0003-4127-8765. Email: hqin@dlut.edu.cn.

[4]School of Civil Engineering, Shijiazhuang Tiedao Univ., Shijiazhuang, Hebei 050043, China. ORCID: https://orcid.org/0000-0003-3166-7644

Note. This manuscript was submitted on May 27, 2020; approved on November 3, 2020; published online on January 4, 2021. Discussion period open until June 4, 2021; separate discussions must be submitted for individual papers. This paper is part of the ***Journal of Engineering Mechanics***, © ASCE, ISSN 0733-9399.

on structure-dependent algorithms by introducing different control parameters in the integration parameters that are similar in form to that of the CR algorithm to govern the numerical properties of algorithms, including the explicit pseudodynamic algorithm by Chang (2013), Gui's family algorithms by Gui et al. (2014), KR-α algorithms by Kolay and Ricles (2014), and generalized CR algorithms by Fu et al. (2019). Meanwhile, some other types of explicit structure-dependent integration algorithms are proposed for linear and nonlinear structural dynamics. Rezaiee-Pajand and Hashemian (2016) developed a new algorithm with second-order accuracy and unconditional stability. The displacement and velocity increments of this algorithm are defined in terms of the accelerations of two previous time steps, and three integration parameters were introduced to control the stability and numerical dissipation of the procedure. Tang and Lou (2017, 2018) presented a new type of explicit integration algorithm (referred to as the TL algorithm in this paper) for RTHS using a bilinear transformation from a continuous domain to a discrete domain associating with pole-matching based on the control theory. In the TL algorithm, two structure-dependent integration parameters are introduced only in the displacement increment, and favorable characteristics such as unconditional stability for linear systems and second-order accuracy can be achieved.

In order to pursue more favorable numerical performance of the algorithms, many improvements have been conducted in higher stability limits with respect to the existing algorithms for instantaneous stiffness hardening systems (Chang 2007, 2009; Wang et al. 2018), controllable amount of numerical energy dissipation (Chang 1997; Kim and Lee 2018; Kolay and Ricles 2019), and remedy for amplitude growth (Chang 2016, 2018; Li et al. 2020). However, the issue of numerical dispersion of integration algorithms has been paid little attention in the previous studies. In general, period error (PE) is utilized as an index for assessing the numerical dispersion of an integration algorithm. A large amount of PE will seriously decrease solution accuracy and distort the whole simulation procedure, especially for the algorithm employed in conjunction with a large time step.

In this study, a family of explicit structure-dependent integration algorithms with controllable numerical dispersion, named TL-φ algorithms, whose displacement and velocity increments are inherited from the TL algorithm but possess different integration parameters, are proposed and investigated thoroughly with respect to their stability and accuracy properties. By using a precorrected bilinear transformation from a continuous domain to a discrete domain, two integration parameters in the displacement increment are determined according to pole-matching based on the control theory. An additional coefficient φ, related to the critical frequency ω_c of the system, is introduced in the integration parameters of the proposed family of algorithms. The effect of φ on the stability and accuracy of the method is fully assessed. It is shown that the stability characteristics of the proposed family of algorithms are quite similar to the TL algorithm, which is unconditionally stable for linear systems while conditionally stable for nonlinear systems. Meanwhile, the TL-φ algorithms provide much more desirable performance of numerical dispersion for a certain structural natural frequency when compared to other well-developed algorithms. Four numerical examples with different structural properties are presented to demonstrate the validity of the TL-φ algorithms in reducing the undesired large amount of period errors. Actually, the precorrected bilinear transformation and coefficient φ introduced in this paper are also suitable for improving the numerical dispersion behaviors of the other explicit structure-dependent integration algorithms, such as the CR algorithm.

Development of a New Family of Explicit Integration Algorithms

Single Degree-of-Freedom Systems

The EOM for a single degree-of-freedom (SDOF) system with linear elastic behavior can be expressed as (Clough and Penzien 2011; Butcher 2003)

$$m\ddot{u}(t) + c\dot{u}(t) + ku(t) = f(t) \tag{1}$$

where m, c, and k = mass, viscous damping, and stiffness, respectively; $\ddot{u}$, $\dot{u}$, and u = acceleration, velocity, and displacement, respectively; and f = external force. An integration algorithm can be utilized to solve Eq. (1) and the formulation of the TL algorithm can be written in discrete form as (Tang and Lou 2017)

$$m\ddot{u}_{i+1} + c\dot{u}_{i+1} + ku_{i+1} = f_{i+1} \tag{2}$$

$$u_{i+1} = u_i + \alpha_1 \Delta t \dot{u}_i + \alpha_2 \Delta t^2 \ddot{u}_i \tag{3}$$

$$\dot{u}_{i+1} = \dot{u}_i + \Delta t \ddot{u}_i \tag{4}$$

where $\ddot{u}_{i+1}$, $\dot{u}_{i+1}$, and u_{i+1} = acceleration, velocity, and displacement at $(i+1)$th time step, respectively; f_{i+1} = external exciting force at $(i+1)$th time step; Δt = integration time step; and $\alpha_1 \alpha_2$ = integration parameters, which will be determined with the aid of continuous and discrete transfer functions and a pole-matching role based on the control theory (Xia 2018).

Continuous Transfer Function

Assuming at-rest initial conditions, the continuous transfer function $G(s)$ that relates the external excitation $f(t)$ to the displacement $u(t)$ is

$$G(s) = \frac{U(s)}{F(s)} = \frac{1}{m(s^2 + 2\xi\omega_n s + \omega_n^2)} \tag{5}$$

where s = variable in the s domain; and $U(s)$ $F(s)$ are Laplace transforms of $u(t)$ and $f(t)$, respectively.

The solution for s that renders the denominator of $G(s)$ equal to zero is referred to as a pole of the continuous transfer function, and the poles in Eq. (5) are complex variables as

$$s_{1,2} = -\xi \cdot \omega_n \pm i \cdot \sqrt{1-\xi^2} \cdot \omega_n \tag{6}$$

where i = designation for $\sqrt{-1}$.

The stability of $G(s)$ is determined by the position of its poles in the complex s domain. Stable behavior occurs when the poles are located in the left-half plane, near or on the imaginary axis (underdamped, with $0 \le \xi < 1$), and stable exponential decays when the poles are on the negative real axis (overdamped, with $\xi \ge 1$). In contrast, unstable behavior occurs when the poles are located in the right half-plane (negative damping, with $\xi < 0$).

Discrete Transfer Function

For a discrete system, the Z transform of Eqs. (2)–(4) can be derived based on the real translation theorem as (Ogata 2014)

$$m\ddot{U}(z) + c\dot{U}(z) + kU(z) = F(z) \tag{7}$$

$$U(z) = z^{-1}U(z) + \alpha_1 z^{-1}\Delta t\dot{U}(z) + \alpha_2 z^{-1}\Delta t^2 \ddot{U}(z) \tag{8}$$

$$\dot{U}(z) = z^{-1}\dot{U}(z) + z^{-1}\Delta t\ddot{U}(z) \tag{9}$$

Table 1. Coefficients of discrete transfer function of the proposed algorithm for SDOF system

Numerator		Denominator	
n_2	0	d_2	m
n_1	$\alpha_2\Delta t^2$	d_1	$m(\alpha_2\Omega^2+2\xi\Omega-2)$
n_0	$(\alpha_1-\alpha_2)\Delta t^2$	d_0	$m[(\alpha_1-\alpha_2)\Omega^2-2\xi\Omega+1]$

in which z = variable in the z domain; and $\ddot{U}(z)$, $\dot{U}(z)$, $U(z)$, and $F(z)$ = Z transform of $\ddot{u}_{i+1}$, $\dot{u}_{i+1}$, u_{i+1}, and f_{i+1}, respectively.

Substituting Eqs. (8) and (9) into Eq. (7), the discrete transfer function $G(z)$ that relates the external excitation f_{i+1} to the displacement u_{i+1} can be derived as shown in Eq. (10) and Table 1

$$G(z)=\frac{U(z)}{F(z)}=\frac{n_2z^2+n_1z+n_0}{d_2z^2+d_1z+d_0} \tag{10}$$

where n_r and d_r ($r=0,1,2$) = coefficients of the numerator and denominator; ξ = viscous damping ratio; and $\Omega=\omega_n\cdot\Delta t=\sqrt{(k_0)/m}\cdot\Delta t$, ω_n is the natural frequency of the system determined from the initial stiffness k_0.

The stability of the discrete system is also determined by its poles, i.e., the solution for z of the characteristic equation of $G(z)$ in Eq. (10). If $G(z)$ has all of its poles located inside, or on the unit circle in the z domain, the system is stable; otherwise it is unstable (Ogata 2014). The characteristic equation of $G(z)$ is

$$z^2+(\alpha_2\Omega^2+2\xi\Omega-2)z+[(\alpha_1-\alpha_2)\Omega^2-2\xi\Omega+1]=0 \tag{11}$$

Discretization in Control Theory

Discretization of a continuous system can be done by discretizing the continuous system with a desired time step and then solving the responses of the corresponding discrete system. To ensure that the responses of the discrete system can inherit from that of the original continuous system, a specific mapping rule should be followed with respect to the poles of the two systems. A discretization method named Tustin's method, also called the bilinear transformation method, is utilized in control theory for the mapping of poles from the continuous s domain to the discrete z domain (Ogata 2014). According to Tustin's method, the following mapping relationship between s and z is expressed as

$$s=\frac{2}{\Delta t}\frac{z-1}{z+1} \tag{12}$$

By using Eq. (12), the stability property and the frequency characteristics in the s domain are maintained in the process of discretization. Fig. 1 shows the mapping of the stability regions from the continuous system to the discrete system for bilinear transformation. In the figure, the two shadows (position of the poles with respect to stability) indicate that the left half-plane in the s domain is mapped to the unit circle in the z domain, and the discrete system described with this mapped transformation has to have poles inside or on the unit circle in the z domain in order to be stable (Rustemovic and Uzunovic 2018). As s on the imaginary axis maps to z on the unit circle, it has

$$\omega_A=\frac{2}{\Delta t}\tan\left(\frac{\omega_D\Delta t}{2}\right)\quad or\quad \omega_D=\frac{2}{\Delta t}\arctan\left(\frac{\omega_A\Delta t}{2}\right) \tag{13}$$

where ω_A and ω_D = frequencies in the s domain and z domain, respectively.

It is worth noting that $\omega_D\approx\omega_A$ when ω_A is small enough for a specific Δt, indicating that discretization by Tustin's method has small errors in the low-frequency range in comparison to the ideal frequency characteristics. However, the frequency response exhibits large deviations in the high-frequency range, resulting in a nonlinear distortion of ω_A. Therefore, it is necessary to pursue a way to reduce the deviation of the frequency response in comparison to the ideal one, especially for the frequency that dominates the structural dynamics. Based on the bilinear transformation theory, one way of eliminating the nonlinear distortion at the critical frequency $\omega_c=\omega_A$ is to precorrect the relationship of s and z in Eq. (12) by introducing a scaling parameter:

$$\varphi=\frac{\omega_D}{\omega_c}=\frac{\arctan(\frac{\omega_c\Delta t}{2})}{\omega_c}=\frac{\arctan(\Omega/2)}{\Omega/2} \tag{14}$$

where φ = precorrection coefficient that reveals the degree of frequency distortion, $0<\varphi<1$; and $\Omega=\omega_c\Delta t$.

Multiplying the right side of Eq. (12) by Eq. (14), Eq. (12) becomes

$$s=\varphi\frac{2}{\Delta t}\frac{z-1}{z+1} \tag{15}$$

It is noted that when $\varphi=1$, Eq. (15) is reduced to Eq. (12). The introduction of the frequency precorrection is promising as it can ensure that the characteristics of the selected critical frequency in the discrete system are exactly the same as that in the original continuous system. Though nonlinear distortions still exist in other frequencies, the amount of these distortions becomes smaller than that before the precorrection. Substituting Eqs. (14) and (15)

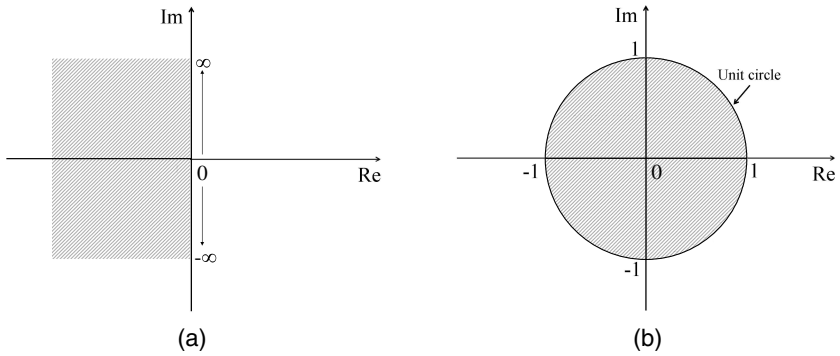

Fig. 1. Schematic of mapping of stability regions from the continuous system to the discrete system: (a) s domain; and (b) z domain.

into Eq. (5), the discrete transfer function $G(z)$ can be rewritten as follows:

$$G(z)=\frac{\Delta t^2(z^2+2z+1)}{m[(\Omega^2+4\xi\Omega\varphi+4\varphi^2)z^2+(2\Omega^2-8\varphi^2)z+\Omega^2-4\xi\Omega\varphi+4\varphi^2]} \tag{16}$$

Then the characteristic equation of Eq. (16) and the poles corresponding to the discrete transfer function $G(z)$ can be expressed as

$$(\Omega^2+4\xi\Omega\varphi+4\varphi^2)z^2+(2\Omega^2-8\varphi^2)z+\Omega^2-4\xi\Omega\varphi+4\varphi^2=0 \tag{17}$$

The poles of Eq. (17) should be the same as that of Eq. (11), so that the integration parameters α_1 and α_2 lead to

$$\begin{aligned}\alpha_1&=\frac{4}{\Omega^2+4\xi\Omega\varphi+4\varphi^2}\\ \alpha_2&=\frac{-2\xi\Omega+4-8\xi^2\varphi+8\xi\varphi(1-\varphi)/\Omega}{\Omega^2+4\xi\Omega\varphi+4\varphi^2}\end{aligned} \tag{18}$$

The algorithms with the displacement and velocity increments as shown in Eqs. (3) and (4) and the integration parameters as given in Eq. (18) are referred to as TL-φ algorithms. It is noted that when $\varphi=1$, the expressions for α_1 and α_2 are identical to those for the TL algorithm (Tang and Lou 2017). Thus, the TL algorithm is a special case ($\varphi=1$) of the proposed family of algorithms.

TL-φ Method for MDOF Systems

For a n-DOF linear elastic system, the EOMs of the system under external excitations and the increments for displacements and velocities are expressed in discrete form as

$$\mathbf{M}\ddot{\mathbf{U}}_{i+1}+\mathbf{C}\dot{\mathbf{U}}_{i+1}+\mathbf{K}\mathbf{U}_{i+1}=\mathbf{F}_{i+1} \tag{19}$$

$$\mathbf{U}_{i+1}=\mathbf{U}_i+\boldsymbol{\alpha}_1\Delta t\dot{\mathbf{U}}_i+\boldsymbol{\alpha}_2\Delta t^2\ddot{\mathbf{U}}_i \tag{20}$$

$$\dot{\mathbf{U}}_{i+1}=\dot{\mathbf{U}}_i+\Delta t\ddot{\mathbf{U}}_i \tag{21}$$

where $\mathbf{M}$, $\mathbf{C}$, and $\mathbf{K}$ = mass, viscous damping, and stiffness matrix, $n\times n$, respectively; $\ddot{\mathbf{U}}$, $\dot{\mathbf{U}}$, and $\mathbf{U}$ = acceleration, velocity, and displacement vector, $n\times 1$, respectively; $\mathbf{F}$ = external force vector, $n\times 1$; and $\boldsymbol{\alpha}_1\boldsymbol{\alpha}_2$ = integration parameter matrices, $n\times n$.

For simplicity, $\mathbf{C}$ is supposed to be proportional and the orthogonality of modes is available in the following equations (Clough and Penzien 2011). For a linear MDOF system, Eqs. (19)–(21) are rewritten in the modal coordinate system as

$$\mathbf{M}^*\ddot{\mathbf{Y}}_{i+1}+\mathbf{C}^*\dot{\mathbf{Y}}_{i+1}+\mathbf{K}^*\mathbf{Y}_{i+1}=\mathbf{F}^*_{i+1} \tag{22}$$

$$\mathbf{Y}_{i+1}=\mathbf{Y}_i+\boldsymbol{\alpha}_1^*\Delta t\dot{\mathbf{Y}}_i+\boldsymbol{\alpha}_2^*\Delta t^2\ddot{\mathbf{Y}}_i \tag{23}$$

$$\dot{\mathbf{Y}}_{i+1}=\dot{\mathbf{Y}}_i+\Delta t\ddot{\mathbf{Y}}_i \tag{24}$$

in which $\boldsymbol{\Phi}=[\boldsymbol{\phi}_1\quad\boldsymbol{\phi}_2\quad\cdots\quad\boldsymbol{\phi}_n]$ is the modal matrix derived from solving the eigenvalue problem, $n\times n$; $\mathbf{M}^*=\boldsymbol{\Phi}^{\mathrm{T}}\mathbf{M}\boldsymbol{\Phi}$, $\mathbf{C}^*=\boldsymbol{\Phi}^{\mathrm{T}}\mathbf{C}\boldsymbol{\Phi}$, and $\mathbf{K}^*=\boldsymbol{\Phi}^{\mathrm{T}}\mathbf{K}\boldsymbol{\Phi}$ are the modal mass matrix, modal diagonal damping matrix, and modal diagonal stiffness matrix, $n\times n$, respectively; $\ddot{\mathbf{Y}}$, $\dot{\mathbf{Y}}$, and $\mathbf{Y}$ are the acceleration, velocity, and displacement vector in modal coordinates, $n\times 1$, respectively; $\mathbf{Y}=\boldsymbol{\Phi}^{-1}\mathbf{U}$; and $\boldsymbol{\alpha}_1^*=\boldsymbol{\Phi}^{-1}\boldsymbol{\alpha}_1\boldsymbol{\Phi}\,\boldsymbol{\alpha}_2^*=\boldsymbol{\Phi}^{-1}\boldsymbol{\alpha}_2\boldsymbol{\Phi}$ are diagonal matrices of integration parameters in the modal coordinate system, $n\times n$.

Eqs. (22)–(24) represent n uncoupled simultaneous equations, and the integration parameter for each mode can be determined based on the one for SDOF system presented in Eq. (18) as follows:

$$\begin{aligned}\alpha_{1j}^*&=\frac{4M_j^*}{4\varphi^2M_j^*+2\varphi\Delta tC_j^*+\Delta t^2K_j^*}\\ \alpha_{2j}^*&=\frac{4M_j^*-\Delta tC_j^*-2\varphi D_j^{*2}+E_j^*}{4\varphi^2M_j^*+2\varphi\Delta tC_j^*+\Delta t^2K_j^*}\end{aligned} \tag{25}$$

where α_{1j}^* and α_{2j}^* = modal integration parameter for the jth mode; M_j^*, C_j^*, and K_j^* = modal mass, damping, and stiffness for the jth mode, respectively; $D_j^*=M_j^{*-1}\cdot C_j^*\cdot K_j^{*-1}\cdot M_j^*$; and $E_j^*=4\varphi(1-\varphi)\Delta tC_j^*\cdot K_j^{*-1}$. Then, the matrices of integration parameters can be expressed as

$$\begin{aligned}\boldsymbol{\alpha}_1&=4\mathbf{B}^{-1}\cdot\mathbf{M}\\ \boldsymbol{\alpha}_2&=\mathbf{B}^{-1}\cdot(4\mathbf{M}-\Delta t\mathbf{C}-2\varphi\mathbf{D}+\mathbf{E})\end{aligned} \tag{26}$$

where $\mathbf{B}=4\varphi^2\cdot\mathbf{M}+2\varphi\Delta t\cdot\mathbf{C}+\Delta t^2\cdot\mathbf{K}$; $\mathbf{D}=(\boldsymbol{\Phi}^T)^{-1}\cdot\mathbf{D}^{*2}\cdot\boldsymbol{\Phi}^{-1}$; and $\mathbf{E}=(\boldsymbol{\Phi}^T)^{-1}\cdot\mathbf{E}^*\cdot\boldsymbol{\Phi}^{-1}$.

For a linear MDOF system, the fundamental frequency ω_1 has a great impact on structural dynamics, so that ω_1 is deemed to be the critical frequency, i.e., $\omega_c=\omega_1$, $\varphi=[\arctan(\Omega_1/2)]/(\Omega_1/2)$, and $\Omega_1=\omega_1\Delta t$ in the following study. It should be noted that φ can be distinct for each mode, and then the constant φ should be replaced by the diagonal matrix $\boldsymbol{\varphi}$, where the elements φ_i of the main diagonal are calculated by ω_i for the ith mode.

Stability Analysis

An integration algorithm is deemed to be unconditionally stable when the free-vibration responses of a SDOF system subjected to any arbitrary initial conditions do not grow without bounds even for large value time steps (Clough and Penzien 2011). The stability of the TL-φ algorithms is discussed in this section, and it is illustrated that the proposed method is unconditionally stable only for linear systems but conditionally stable for nonlinear systems.

Linear Systems

According to the algorithm stability analysis theory, the stability of an integration algorithm applied to the linear elastic system can be conducted by looking at the amplification matrix $\mathbf{A}$ as follows (Yu and Zou 2016; Clough and Penzien 2011):

$$[u_{i+1},\Delta t\dot{u}_{i+1},\Delta t^2\ddot{u}_{i+1}]^T=\mathbf{A}[u_i,\Delta t\dot{u}_i,\Delta t^2\ddot{u}_i]^T \tag{27}$$

where $\mathbf{A}$ is determined by

$$\mathbf{A}=\begin{bmatrix}1 & \alpha_1 & \alpha_2\\ 0 & 1 & 1\\ -\Omega^2 & -2\xi\Omega-\alpha_1\Omega^2 & -2\xi\Omega-\alpha_2\Omega^2\end{bmatrix} \tag{28}$$

To ensure a bounded response by the integration algorithm, the spectral radius of the amplification matrix should satisfy the stability condition of

$$\rho(\mathbf{A})=\max(|\lambda_1|,|\lambda_2|,|\lambda_3|)\le 1 \tag{29}$$

where $\rho(\mathbf{A})$ and $\lambda_i(i=1,2,3)$ = spectral radius and eigenvalues of $\mathbf{A}$. The eigenvalues λ_i can be determined by solving the following eigenvalue problem:

$$|\mathbf{A}-\lambda\mathbf{I}|=\lambda^3-2A_1\lambda^2+A_2\lambda-A_3=0 \tag{30}$$

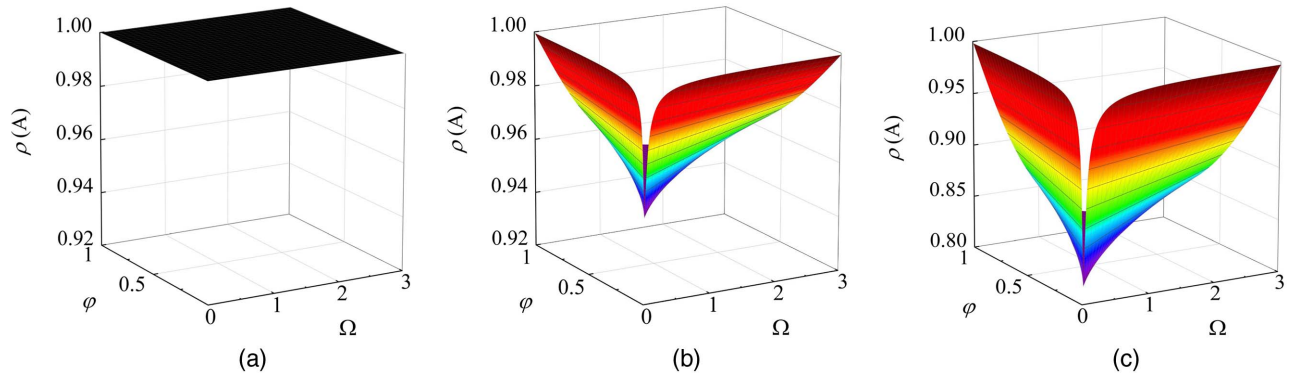

Fig. 2. Spectral radius for TL-φ algorithms for different values of ξ for linear elastic system: (a) $\xi = 0.0$; (b) $\xi = 0.05$; and (c) $\xi = 0.2$.

where $\mathbf{I}$ = identity matrix; A_1 = trace of $\mathbf{A}$; A_2 = sum of principal minors of $\mathbf{A}$; and $A_3 = 0$ is the determinant of $\mathbf{A}$.

Variations of the spectra radius $\rho(\mathbf{A})$ with Ω and φ for different values of ξ are plotted in Fig. 2. The figures show that $\rho(\mathbf{A})$ is always less than or equal to unity for any φ in the range of $0 \le \varphi \le 1$ and $\xi \ge 0$, indicating an unconditional stability of the TL-φ algorithms when used for linear systems.

Nonlinear Systems

Unconditional stability of an integration algorithm in linear systems may not remain so when the system presents nonlinear structural behaviors (Chen and Ricles 2008b). Hence, it is necessary to study the stability characteristics of the proposed method when applied to nonlinear systems. For a nonlinear SDOF system, the discrete EOM in Eq. (2) can be written in the following incremental form:

$$m\Delta\ddot{u}_i + c\Delta\dot{u}_i + \Delta r_i = \Delta f_i \tag{31}$$

The increments of acceleration $\Delta\ddot{u}_i$, velocity $\Delta\dot{u}_i$ and external excitation Δf_i are defined as $\Delta\ddot{u}_i = \ddot{u}_{i+1} - \ddot{u}_i$, $\Delta\dot{u}_i = \dot{u}_{i+1} - \dot{u}_i$, and $\Delta u_i = u_{i+1} - u_i$. For a small value of Δt, the increment of restoring force Δr_i can be approximated as (Clough and Penzien 2011)

$$\Delta r_i = r_{i+1} - r_i = k_{i+1}\Delta u_i \tag{32}$$

where k_{i+1} = stiffness at the $(i+1)$th time step; and Δu_i = increment of displacement defined as $\Delta u_i = u_{i+1} - u_i$. Substituting Eq. (32) into Eq. (31) leads to

$$m\Delta\ddot{u}_i + c\Delta\dot{u}_i = \Delta f_i - \Delta r_i = \Delta f_i - k_{i+1}\Delta u_i = \Delta l_i \tag{33}$$

Eq. (33) can also be represented by a closed-loop block diagram in the z domain as shown in Fig. 3. In the figure, $\Delta F(z)$, $F(z)$, $\Delta U(z)$, and $\Delta L(z)$ are the Z transform of Δf_i, f, Δu_i, and Δl_i; $H(z)$ is a transfer function that relates $\Delta F(z)$ to $F(z)$, and $G'(z)$ is an open-loop transfer function that relates $\Delta U(z)$ to

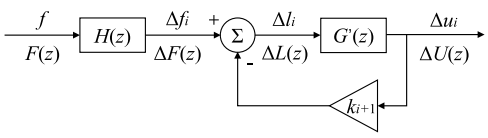

Fig. 3. Closed-loop block diagram representation of TL-φ algorithms under nonlinear structural behavior.

$\Delta L(z)$ by using the TL-φ algorithms. The discrete transfer functions $H(z)$ and $G'(z)$ can be derived as

$$H(z) = \frac{\Delta F(z)}{F(z)} = \frac{z-1}{z} \tag{34}$$

$$G'(z) = \frac{\Delta U(z)}{\Delta L(z)} = \frac{\alpha_2\Delta t^2 z + (\alpha_1 - \alpha_2)\Delta t^2}{mz^2 + (c\Delta t - 2m)z + m - c\Delta t} \tag{35}$$

The closed-loop transfer function $G_{cl}(z)$ that relates $\Delta U(z)$ to $\Delta F(z)$ and the corresponding characteristic equation are

$$G_{cl}(z) = \frac{\Delta U(z)}{\Delta F(z)} = \frac{G'(z)}{1 + k_{i+1}G'(z)} \tag{36}$$

$$1 + k_{i+1}G'(z) = 0 \tag{37}$$

The stability of the discrete closed-loop transfer function $G_{cl}(z)$ in Eq. (36) is determined by its pole positions in the z plain. Substituting Eq. (35) into Eq. (37), Eq. (37) can be rewritten as

$$1 + k_{i+1}\frac{\alpha_2\Delta t^2 z + (\alpha_1 - \alpha_2)\Delta t^2}{mz^2 + (c\Delta t - 2m)z + m - c\Delta t} = 0 \tag{38}$$

Eq. (38) can be used to evaluate the stability of the TL-φ method with different values of φ, in which the solutions of z for various values of k_{i+1} can conveniently be obtained using a root locus approach (Wang et al. 2008) in accordance with the open-loop transfer function $G'(z)$. Based on the definition for the root locus, if all of the possible poles of the closed-loop transfer function G_{cl} fall on or within the unite circle, the integration algorithm will be stable for nonlinear structural behavior. The root loci of $k_{i+1}G'(z)$ for the TL-φ method with $\varphi = 0.05$, 0.5, 0.75, and 1.0 when applied to a nonlinear SDOF system are plotted in Fig. 4 for $\Delta t = 0.02$ s, $\omega_n = \pi$ rad/s, and $\xi = 0.02$. It can be observed that as k_{i+1} increases from 0 to ∞, two branches of the root loci originate at open-loop poles and end at open-loop zeros. In general, one of the root loci branches that originates at an open-loop pole ends at an open-loop zero, while the remaining branch goes to infinity, which means that the proposed family of algorithms is only stable for a finite range of stiffness values. For $0 < \varphi < 1$, the root loci plot crosses the unite circle at $z = -1$, while for $\varphi = 1$, two branches with complex conjugate roots leave the unite circle somewhere between $z = 1$ and $z = -1$.

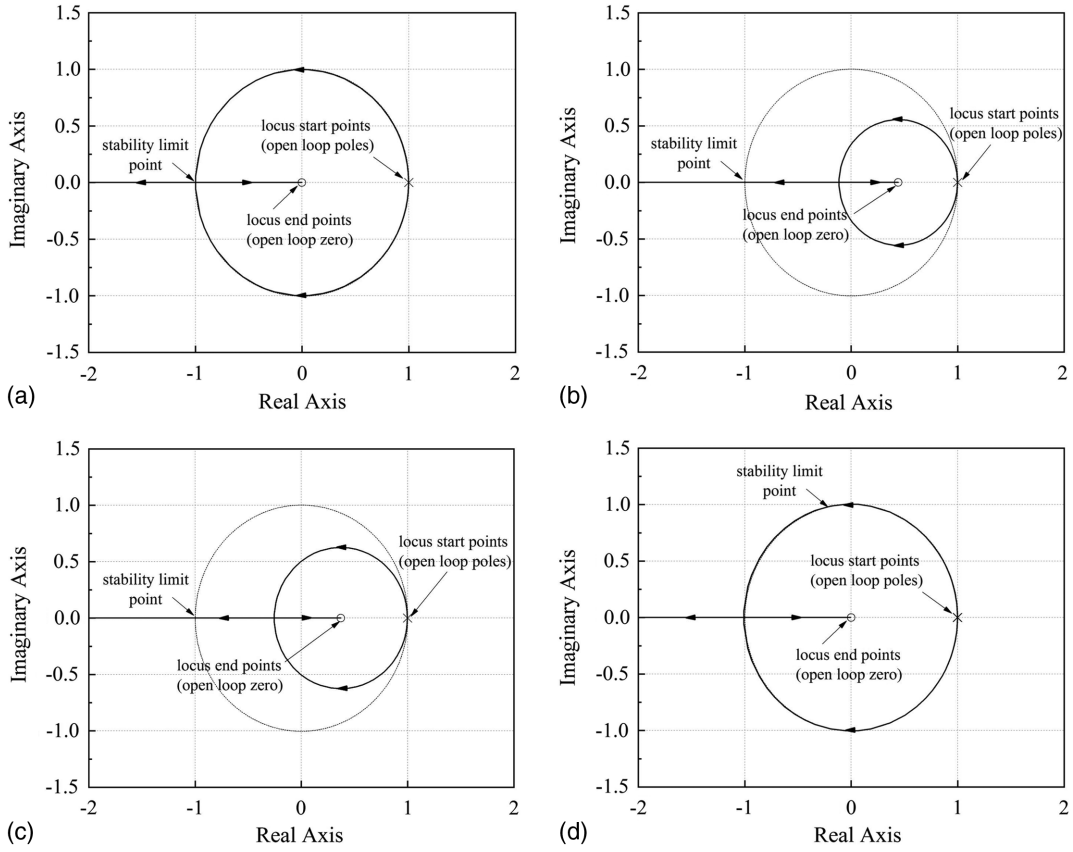

Fig. 4. Root locus of open-loop transfer function $H(z)G'(z)$ of TL-φ method with different φ: (a) $\varphi = 0.05$; (b) $\varphi = 0.5$; (c) $\varphi = 0.75$; and (d) $\varphi = 1.0$.

It is of great interest to study the upper stability limit $[\Omega]$ for the proposed algorithms when applied to nonlinear systems. For $0 < \varphi < 1$, the solution of k_{i+1} for $[\Omega]$ can conveniently be solved by substituting $z = -1$ into Eq. (38), which leads to

$$k_{i+1} \le \frac{4m - 2c\Delta t}{(2\alpha_2 - \alpha_1)\Delta t^2} \quad or \quad \frac{k_{i+1}}{k_0} \le \frac{4m - 2c\Delta t}{m\Omega_0^2(2\alpha_2 - \alpha_1)} \tag{39}$$

When $\varphi = 1$, the expressions for the integration parameters α_1 and α_2 are identical to that of the TL algorithm. The stability behavior of the TL algorithm for nonlinear systems can still be discussed by solving the characteristic equation for the amplification matrix. This is different from Eq. (28), in which the amplification matrix $\mathbf{A}_{i+1}$ remains invariant for each time step, i.e., $\mathbf{A}_{i+1} = \mathbf{A}$, for a linear system, whereas it is generally varies for a nonlinear system. That is

$$\mathbf{A}_{i+1} = \begin{bmatrix} 1 & \alpha_1 & \alpha_2 \\ 0 & 1 & 1 \\ -\Omega_{i+1}^2 & -2\xi\Omega_0 - \alpha_1\Omega_{i+1}^2 & -2\xi\Omega_0 - \alpha_2\Omega_{i+1}^2 \end{bmatrix} \tag{40}$$

The eigenvalues $\lambda_{1,2,3}$ can still be derived by solving the eigenvalue problem as shown in Eq. (30), where

$$\begin{aligned} A_1 &= 1 - \frac{1}{D}[(\xi\Omega_0^2 + 4\xi^2\Omega_0 + 4\xi)\Omega_0 + (2 - 4\xi^2 - \xi\Omega_0)\Omega_{i+1}^2] \\ A_2 &= 1 - \frac{1}{D}[(2\xi\Omega_0^2 + 8\xi^2\Omega_0 + 8\xi)\Omega_0 - (8\xi^2 + 2\xi\Omega_0)\Omega_{i+1}^2] \\ A_3 &= 0 \end{aligned} \tag{41}$$

where $D = \Omega_0^2 + 4\xi\Omega_0\varphi + 4\varphi^2$, $\Omega_0 = \sqrt{k_0/m} \cdot \Delta t$, $\Omega_{i+1} = \sqrt{k_{i+1}/m} \cdot \Delta t$, and k_0 = initial stiffness while k_{i+1} = stiffness at the end of the $(i+1)$th time step. In general, the stability conditions can be found from the reference Belytschko and Hughes (1983), which are:

$$\begin{cases} -1 \le A_2 \le 1 \\ -(A_2 + 1) \le A_1 \le (A_2 + 1) \end{cases} \quad or \quad \begin{cases} A_2 = 1 \\ -2 \le A_1 \le 2 \end{cases} \tag{42}$$

Two types of nonlinear structural behaviors are considered in accordance with the relation of k_{i+1} and k_0, namely, instantaneous softening stiffness for $0 < \delta_{i+1} = k_{i+1}/k_0 < 1$ and instantaneous hardening stiffness for $\delta_{i+1} > 1$, where δ is instantaneous degree of nonlinearity. Fig. 5 shows the variations of the upper stability limit $[\Omega]$ with an increase of δ for different values of ξ and φ. In the figures, $\delta_{i+1} = 1$ means that the stiffness at the end of the $(i+1)$th time step k_{i+1} is equal to the initial stiffness k_0, representing for a linear elastic system. It is illustrated that the TL-φ algorithm is unconditionally stable only for instantaneous softening stiffness systems with zero viscous damping, and it is conditionally stable for instantaneous hardening stiffness systems and instantaneous softening stiffness systems with nonzero viscous damping. The upper stability limit $[\Omega]$ decreases with the decrease of φ for all δ and ξ, and it decreases with an increasing value of δ_{i+1} for instantaneous hardening stiffness systems while increasing with an increasing δ_{i+1} for instantaneous softening stiffness systems. Meanwhile, the upper stability limit $[\Omega]$ is greatly affected by the viscous damping ξ when $0 < \delta_{i+1} < 1$, as the curves of $[\Omega]$ move down with the increase of ξ.

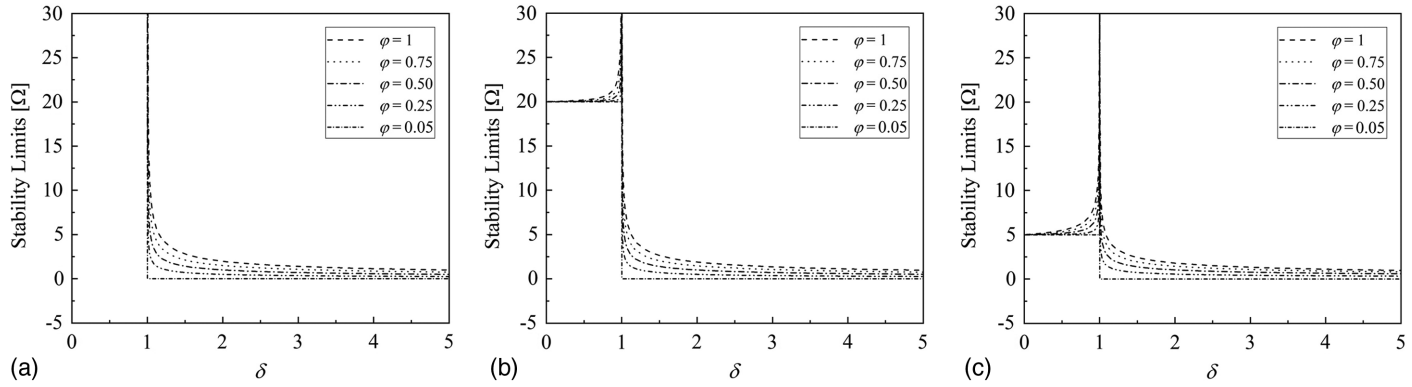

Fig. 5. Variations of upper stability limits with δ for TL-φ algorithms: (a) $\xi = 0.0$; (b) $\xi = 0.05$; and (c) $\xi = 0.20$.

Accuracy Analysis

The accuracy properties of the TL-φ algorithms can be assessed after expressing a pair of complex conjugates at the $(i+1)$th time step as follows (Chopra 2001):

$$\lambda_{1,2} = A_1 \pm i \cdot \sqrt{A_2 - A_1^2} = \exp(-\bar{\xi}_{i+1} \cdot \bar{\Omega}_{i+1} \pm i \cdot \bar{\Omega}_{i+1}^D) \tag{43}$$

where

$$\begin{aligned} & i = \sqrt{-1} \\ & \bar{\Omega}_{i+1} = \bar{\omega}_{i+1} \Delta t \\ & \bar{\Omega}_{i+1}^D = \bar{\Omega}_{i+1} \sqrt{1 - \bar{\xi}^2} = \arctan\left(\sqrt{\frac{A_2}{A_1^2} - 1} \right) \\ & \bar{\xi}_{i+1} = -\frac{\ell n(A_2)}{2\bar{\Omega}_{i+1}} \end{aligned} \tag{44}$$

where $\bar{\xi}_{i+1}$ and $\bar{\omega}_{i+1}$ = numerical damping ratio and numerical frequency related to integration algorithms.

In general, numerical dispersion and energy dissipation characteristics are two indices evaluating the accuracy of an integration algorithm. The former characteristic is usually expressed by the relative period error $\text{PE} = (\bar{T} - T_n)/(T_n) = (\omega_n)/\bar{\omega} - 1$, in which $\bar{T} = 2\pi/\bar{\omega}$, $T_n = 2\pi/\omega_n$ refers to the numerical and natural periods of the systems. The latter one can be expressed by the numerical damping ratio $\bar{\xi}$, which is related to amplitude decay in one cycle of free vibration.

The variations of relative period errors with Ω for the TL-φ algorithms (TL-φ) and three other well-developed algorithms, including the Chang explicit method (Chang), the CR algorithm (CR), and the TL algorithm (TL), are shown in Fig. 6 for different values of φ and ξ. It is illustrated that positive values of PE, which is in correspondence to period elongation, are generally found for all these methods and increase with the increasing of Ω. In this paper, the fundamental frequency ω_1 is deemed to be the critical frequency, so that φ is determined by $\Omega_1 = \omega_1 \Delta t$ as shown in Eq. (14) and the curves for the TL-φ algorithms with a certain value of φ start from the point that corresponds to $\Omega = \Omega_1$. When compared with the Chang explicit method, the CR algorithm, and the TL algorithm, it is clearly seen that the values of PE for the TL-φ algorithms ($\varphi \neq 1$) are much smaller than those of the other three methods for a given Ω. When φ approaches 1, the curves for the TL-φ algorithms, the CR algorithm, and the TL algorithm are overlapped together for any values of ξ. It is also worth noting that the curve for the TL-φ algorithms moves right and slightly down as the value of φ decreases. For a specific Ω larger than Ω_1, the relative period error decreases with the decrease of φe, implying that a larger value of Ω_1 accompanies a smaller period distortion. Furthermore, the values of PE for Ω_1 are equal or near to zero, revealing that the introduction of the precorrection coefficient φ leads to a minimum of the period distortion at the selected critical frequency.

Fig. 7 shows the variations of the numerical damping ratio with Ω for different values of φ and ξ. Fig. 7(a) reveals that there is no numerical dissipation for all the methods when $\xi = 0$, whereas the absolute numerical damping ratio, which corresponds to a negative value, generally increases with Ω when $\xi > 0$. For a given Ω, the absolute numerical damping ratio slightly increases with the decrease of φ, implying that a larger value of Ω_1 accompanies a larger numerical dissipation. Although the decrease of φ may have a negative effect on the numerical dissipation of algorithms, it can significantly improve the numerical dispersion properties of algorithms, especially when the selected critical frequency is higher and the chosen integration step for integration is large.

Numerical Simulation

Four numerical examples are conducted to demonstrate the effectiveness of the controllable numerical dispersion characteristics of the proposed algorithms in reducing undesired period distortion for both linear and nonlinear systems.

Case 1: Free Vibration of a Linear Undamped SDOF System

Free-vibration responses of a linear undamped SDOF system are determined using TL-φ algorithms, the Chang explicit method, the CR algorithm, and the TL algorithm. The structural properties are $m = 10$ kg and $k = 1{,}000$ N/m, and the natural frequency of the system is 10 rad/s, which is deemed to be the critical frequency ω_c in this case. The initial condition of the system is $u_0 = 0$ m and $\dot{u}_0 = 1$ m/s. Two time steps of 0.02 and 0.05 s are adopted for integration, so that for $\Omega = \omega_c \Delta t = 0.2$ and 0.5, $\varphi = 0.997$ and 0.979, respectively. Two error indicators, normalized energy error (NEE) and normalized root-mean-square error (NRMSE), are adopted for accuracy analysis of all four methods and defined as (Fu 2017)

$$\text{NEE} = \left| \frac{\sum_{i=1}^n u_{\text{RM},i}^2 - \sum_{i=1}^n u_{\text{CM},i}^2}{\sum_{i=1}^n u_{\text{CM},i}^2} \right| \tag{45}$$

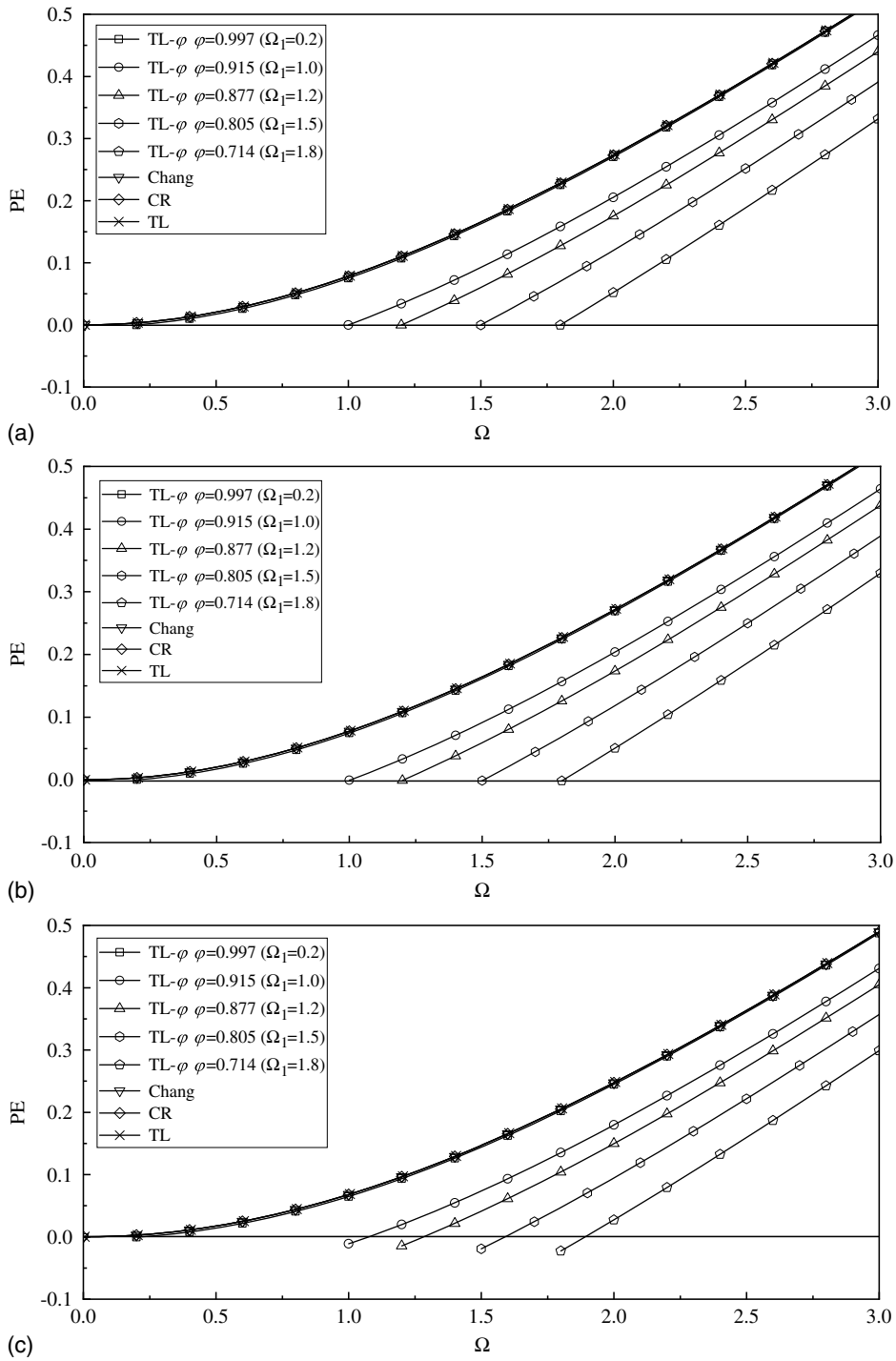

Fig. 6. Relative period errors for TL-φ algorithms with different values of φ and ξ: (a) $\xi = 0.0$; (b) $\xi = 0.05$; and (c) $\xi = 0.20$.

$$\text{NRMSE} = \frac{\sqrt{\sum_{i=1}^{n} \frac{(u_{\text{RM},i} - u_{\text{CM},i})^2}{n}}}{\max(u_{\text{CM},i}) - \min(u_{\text{CM},i})} \tag{46}$$

where subscript CM and RM = computing model and reference model, respectively; and n = number of samples (time steps). In this case, the responses obtained by the four methods are referred to as CM, while the analytical solution from the dynamics of structures (Clough and Penzien 2011) is deemed to be RM. In general, NEE reflects signal energy, which is sensitive to amplitude differences of the dynamic responses while insensitive to frequency differences; on the contrary, NRMSE is sensitive to frequency differences of the dynamic responses while insensitive to amplitude differences.

Table 2 shows the displacement errors between CM and RM for the two selected time steps, respectively. It is shown that the errors of the two indexes for all the methods increase with an increasing value of Δt, indicating that a large time step leads to larger distortions in the responses for both amplitude and period. For a specific Δt, though NEEs for TL-φ algorithms are relatively larger than those for the Chang explicit method and the TL algorithm, NRMSEs for the TL-φ algorithms are significantly smaller than those for the other three methods, revealing a more favorable numerical dispersion

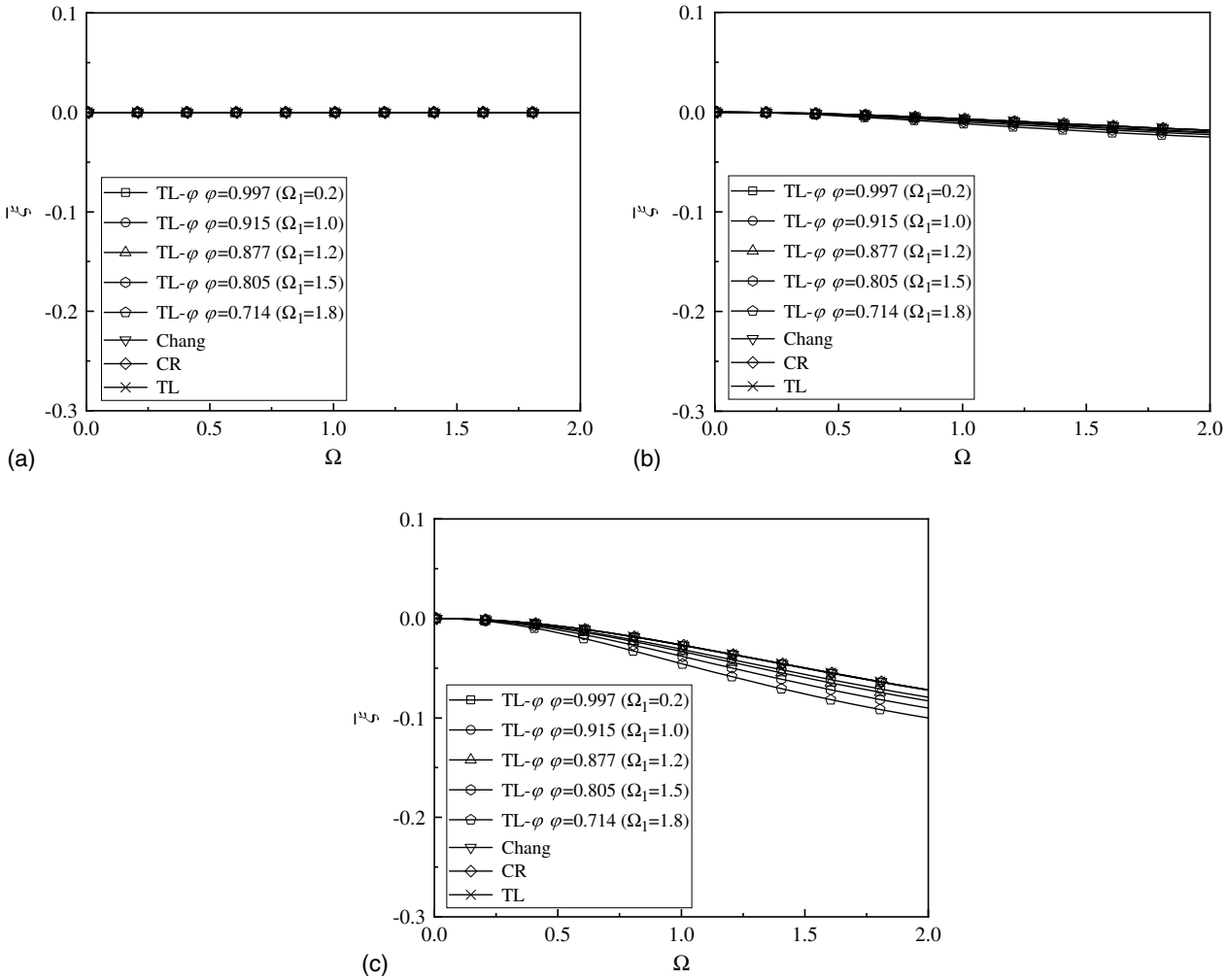

Fig. 7. Numerical damping ratio for TL-φ algorithms with different values of φ and ξ: (a) $\xi = 0.0$; (b) $\xi = 0.05$; and (c) $\xi = 0.20$.

Table 2. Displacement errors of a linear SDOF system under free vibration (%)

Error index	Time step	TL-φ	Chang	CR	TL
NEE	$\Delta t = 0.02$ s	0.67050	0.2929	2.3088	0.2929
	$\Delta t = 0.05$ s	4.3192	0.9059	13.9133	0.9059
NRMSE	$\Delta t = 0.02$ s	0.0593	1.6822	1.7026	1.6822
	$\Delta t = 0.05$ s	0.2394	6.2808	6.5177	6.2808

property by introducing the precorrection coefficient φ that corresponds to the structural properties.

Fig. 8 presents the displacement responses of the forced vibration of the SDOF system obtained by the proposed method, the Chang explicit method, the CR algorithm, and the TL algorithm with two time steps. In each subfigure, *Exact* denotes the responses derived from analytical solutions based on the structural dynamic theory (Clough and Penzien 2011). It is clearly seen in Fig. 8(b) that the curves of TL-φ and Exact are overlapped together when $\Delta t = 0.02$ s, while a certain period elongation appears in the curves of Chang, CR, and TL. When $\Delta t = 0.05$ s as shown in Fig. 8(d), the curve of TL-φ can still match that of Exact well, though a slight difference exists in the amplitude, and the period elongation becomes larger for that of Chang, CR, and TL. The velocity and acceleration responses are also given in Figs. 9 and 10. The conclusion can be drawn that the introduction of the precorrection coefficient φ can diminish the period distortion for the critical frequency and keep a high accuracy in dynamic analysis. For a selected critical frequency, the advantage of the controllable numerical dispersion is more significant when the integration steps are large, which is consistent with the aforementioned statements.

Case 2: Forced Vibration of a Linear SDOF System with Damping

Case 2 is a linear undamped SDOF system with zero initial conditions and subjected to a ground acceleration. The structural properties of $m = 2$ kg, $k = 1{,}000$ N/m and $\xi = 0.01$, $c = 2\xi\sqrt{\text{km}} = 0.8944$ N · s/m. The natural frequency of the system is 22.36 rad/s, and $\Omega_1 = \omega_1 \Delta t = 0.447$ and 0.983, $\varphi = 0.983$ and 0.894 for the time step of 0.02 and 0.05 s, respectively. The ground acceleration is taken as $a_g = 40[\sin(2t) + \sin(3t)]$.

Table 3 shows the displacement errors for the two selected time steps, in which RM is calculated by the Newmark algorithm with $[\gamma, \beta] = [1/2, 1/4]$ and $\Delta t = 0.001$ s in this case. It is seen that the values of the two indexes for all methods increase with an increasing value of Δt. Displacement errors for TL-φ algorithms are still smaller than those for the other three algorithms, indicating an improvement in computational accuracy by introducing the

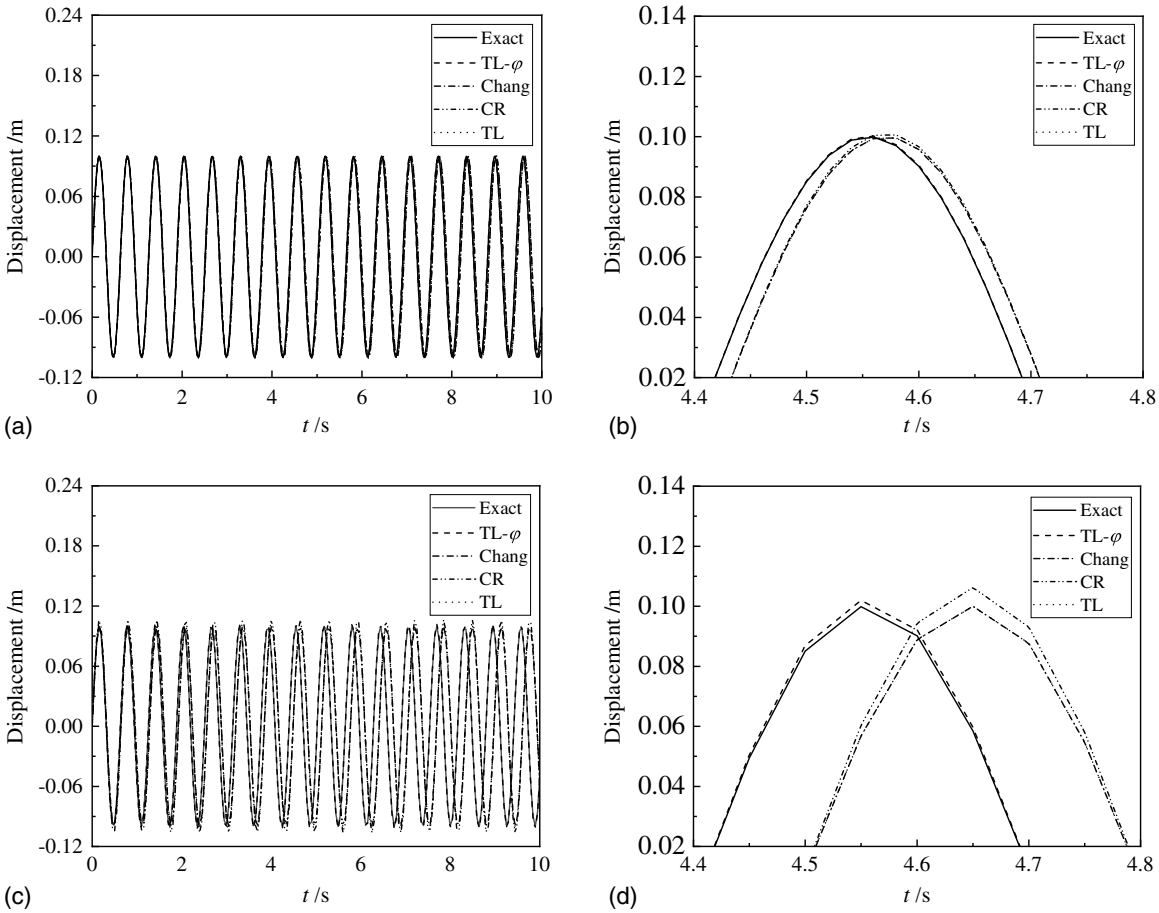

Fig. 8. Displacement responses of free vibration of a linear SDOF system: (a) $\Delta t = 0.02$ s, 0 s $\leq t \leq$ 10 s; (b) $\Delta t = 0.02$ s, 4.4 s $\leq t \leq$ 4.8 s; (c) $\Delta t = 0.05$ s, 0 s $\leq t \leq$ 10 s; and (d) $\Delta t = 0.05$ s, 4.4 s $\leq t \leq$ 4.8 s.

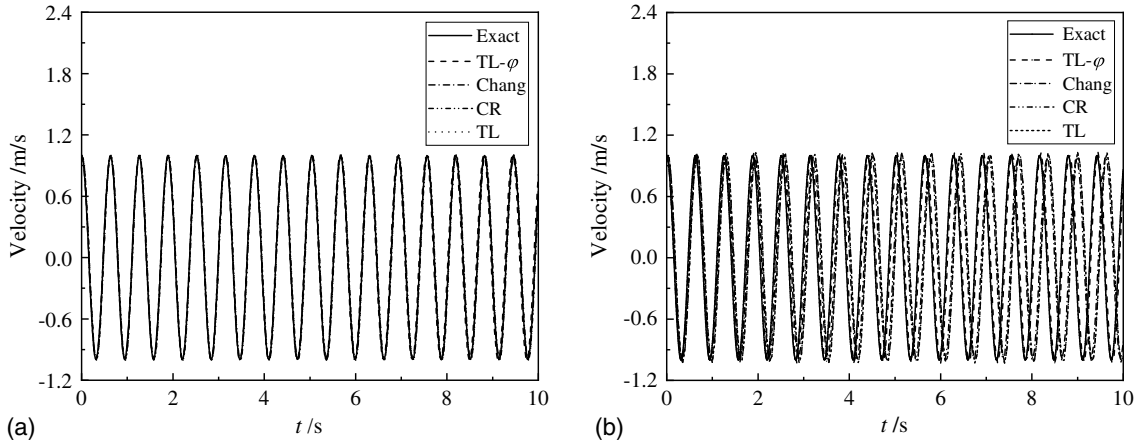

Fig. 9. Velocity responses of free vibration of a linear SDOF system: (a) $\Delta t = 0.02$ s; and (b) $\Delta t = 0.05$ s.

precorrection coefficient φ that corresponds to the structural properties. Fig. 11 presents the displacement responses of the SDOF system obtained by all the methods. It is clearly seen in Fig. 11(b) that the curves of TL-φ and Exact are overlapped together when $\Delta t = 0.02$ s, while a certain period elongation appears in that of Chang, CR, and TL. When $\Delta t = 0.05$ s as shown in Fig. 11(d), the curve of TL-φ can still match that of Exact well, though a little difference exists in the amplitude, and the period elongation becomes larger for that of Chang, CR, and TL. The velocity and acceleration responses are also given in Figs. 12 and 13.

Case 3: Linear MDOF System

A five-story linear elastic shear-type frame structure with zero damping is taken as an example to investigate the efficiency

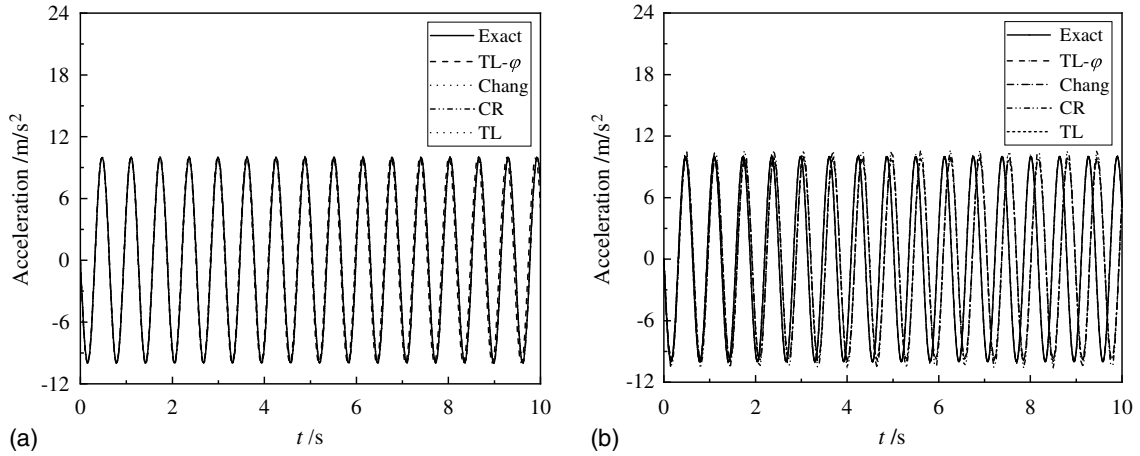

Fig. 10. Acceleration responses of free vibration of a linear SDOF system: (a) $\Delta t = 0.02$ s; and (b) $\Delta t = 0.05$ s.

Table 3. Displacement errors of a linear SDOF system under forced vibration (%)

Error index	Time step	TL-φ	Chang	CR	TL
NEE	$\Delta t = 0.02$ s	0.1589	0.3022	0.3034	0.3022
	$\Delta t = 0.05$ s	1.2401	2.2041	2.2267	2.2030
NRMSE	$\Delta t = 0.02$ s	0.0699	1.0901	1.0893	1.0902
	$\Delta t = 0.05$ s	0.3194	1.6061	1.6081	1.6060

of the proposed method in controlling the numerical dispersion for the MDOF system, as shown in Fig. 14. The initial structural properties are $m = 10^5$ kg and $k = 10^9$ N/m. The natural frequencies of the system are 28.463, 83.083, 130.97, 168.25, and 191.90 rad/s for the five modes, respectively; the normalized modal matrix is given by $\boldsymbol{\Phi} = [\boldsymbol{\phi}_1 \quad \boldsymbol{\phi}_2 \quad \boldsymbol{\phi}_3 \quad \boldsymbol{\phi}_4 \quad \boldsymbol{\phi}_5]$, where $\boldsymbol{\phi}_1 = [0.2846 \quad 0.5462 \quad 0.7653 \quad 0.9190 \quad 1.0000]^T$, $\boldsymbol{\phi}_2 = [0.7653 \quad 1.0000 \quad 0.5462 \quad -0.2846 \quad -0.9190]^T$,

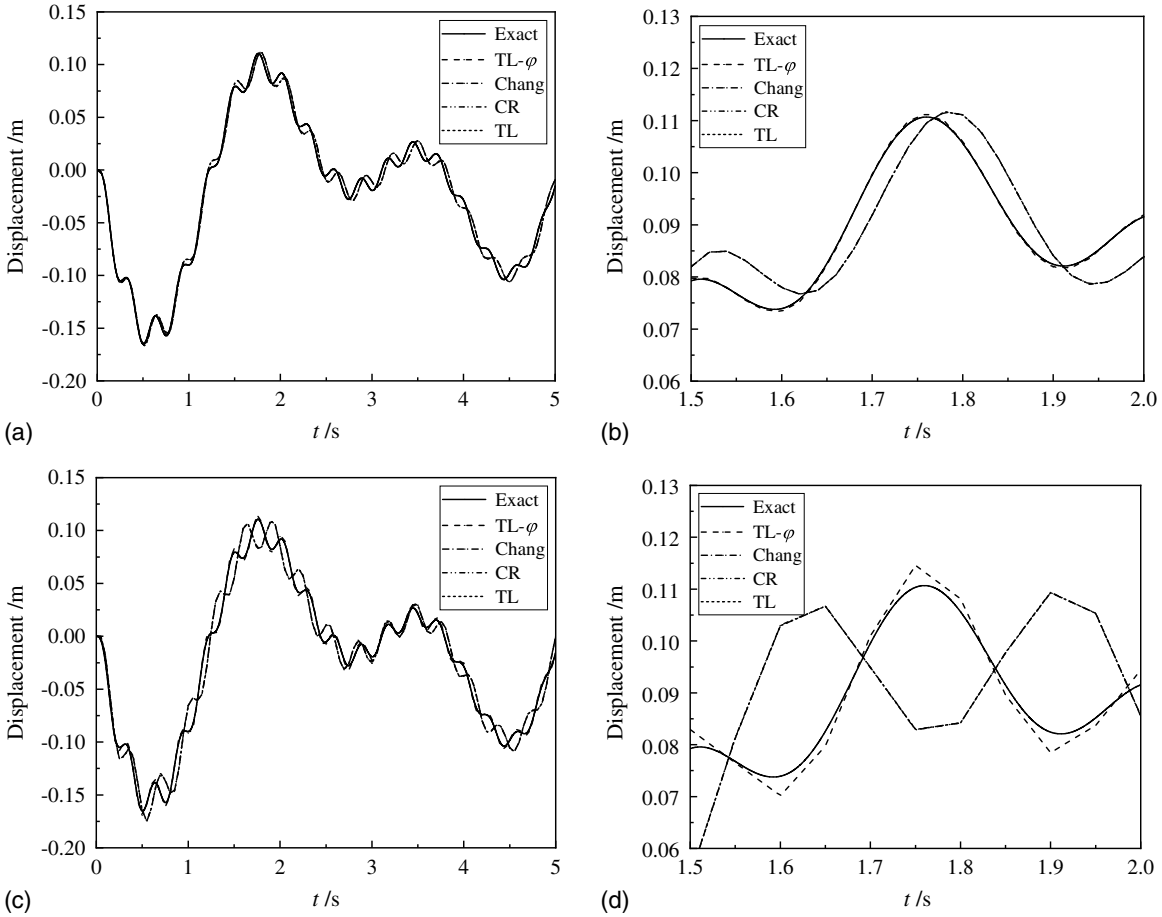

Fig. 11. Displacement responses of free vibration of a linear SDOF system: (a) $\Delta t = 0.02$ s, 0 s $\le t \le$ 5 s; (b) $\Delta t = 0.02$ s, 1.5 s $\le t \le$ 2.0 s; (c) $\Delta t = 0.05$ s, 0 s $\le t \le$ 5 s; and (d) $\Delta t = 0.05$ s, 1.5 s $\le t \le$ 2.0 s.

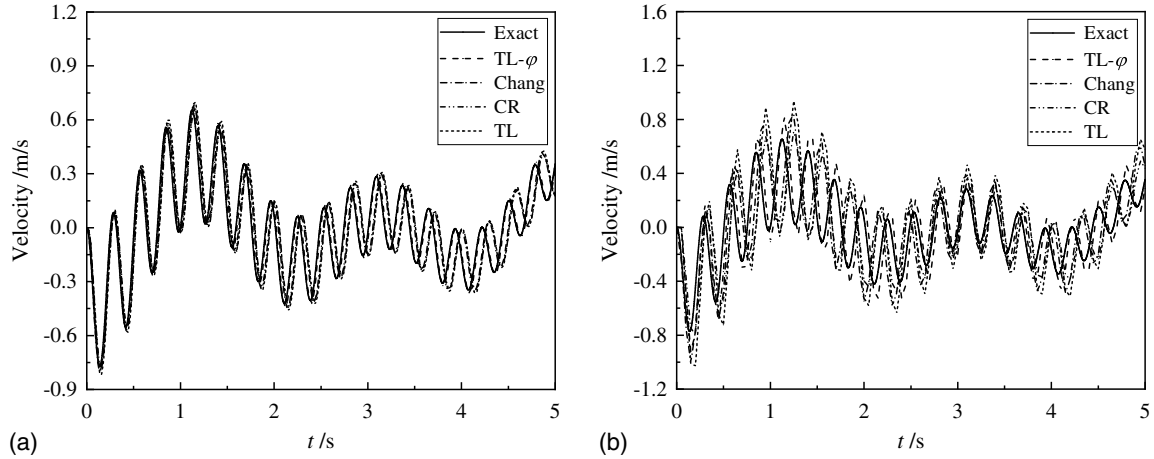

Fig. 12. Velocity responses of forced vibration of a linear SDOF system: (a) $\Delta t = 0.02$ s; and (b) $\Delta t = 0.05$ s.

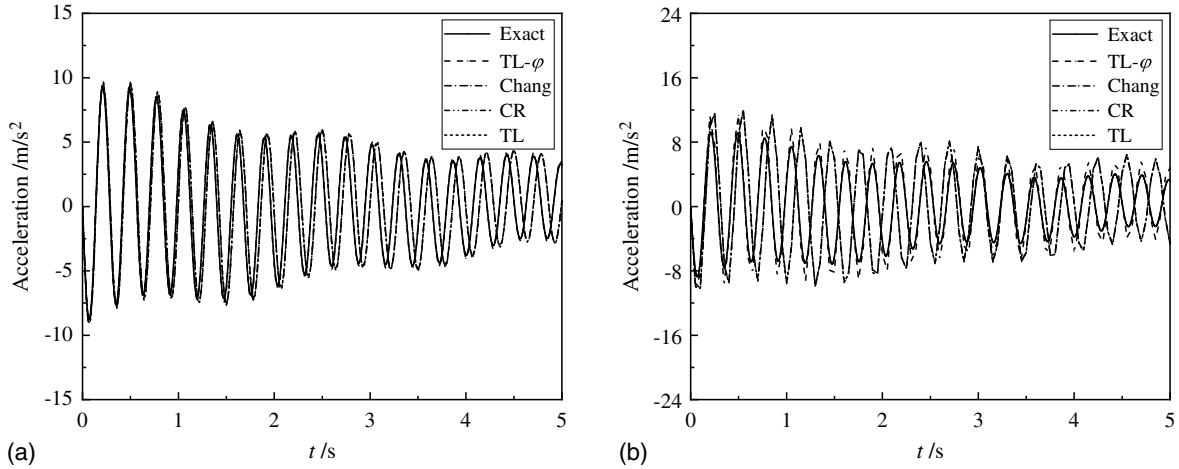

Fig. 13. Acceleration responses of forced vibration of a linear SDOF system: (a) $\Delta t = 0.02$ s; and (b) $\Delta t = 0.05$ s.

$\boldsymbol{\phi}_3 = [\,1.0000 \quad 0.2846 \quad -0.9190 \quad -0.5462 \quad 0.7635\,]^T$, $\boldsymbol{\phi}_4 = [\,0.9190 \quad -0.7653 \quad -0.2846 \quad 1.0000 \quad -0.7562\,]^T$, and $\boldsymbol{\phi}_5 = [\,0.5462 \quad -0.9190 \quad 1.0000 \quad -0.7635 \quad -0.2846\,]^T$.

The dynamic responses of the system subjected to a ground acceleration of $a_g = 80[\sin(2t) + \sin(3t)]$ are obtained from the TL-φ algorithms, the Chang explicit method, the CR algorithm, and the TL algorithm. The integration steps for these four methods are $\Delta t = 0.02$ and 0.05 s, and $\omega_1 = 28.463$ rad/s is chosen as the critical frequency in this case, so that $\varphi = 0.973$ and 0.825 for the TL-φ algorithms, respectively. The reference solutions are calculated using the Newmark algorithm with $[\gamma, \beta] = [1/2, 1/4]$ and $\Delta t = 0.001$ s. The numerical results for the initial conditions of $u_0 = 0$ m, $\dot{u}_0 = 0$ m/s are displayed in the following tables and figures. Table 4 shows that all the displacement errors for the TL-φ algorithms are smaller than those for the other three algorithms, especially the NRMSE that is sensitive to frequency differences of the dynamic responses.

Figs. 15–17 plot the dynamic responses of the top story derived from the five algorithms with two integration steps. It is illustrated that the proposed method is applicable to MDOF systems as well. In Fig. 15, the curves of TL-φ and Exact are still overlapped together when $\Delta t = 0.02$ s, while a certain period elongation appears

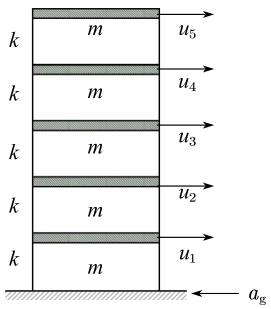

Fig. 14. Schematic diagram of a five-story shear frame building without damping.

Table 4. Displacement errors of a linear MDOF system (%)

Error index		TL-φ	Chang	CR	TL
NEE	$\Delta t = 0.02$ s	0.2382	0.4009	0.4009	0.4009
	$\Delta t = 0.05$ s	2.1222	3.0091	3.0091	3.0091
NRMSE	$\Delta t = 0.02$ s	0.1333	3.0472	3.0472	3.0472
	$\Delta t = 0.05$ s	0.6233	2.5530	2.5530	2.5530

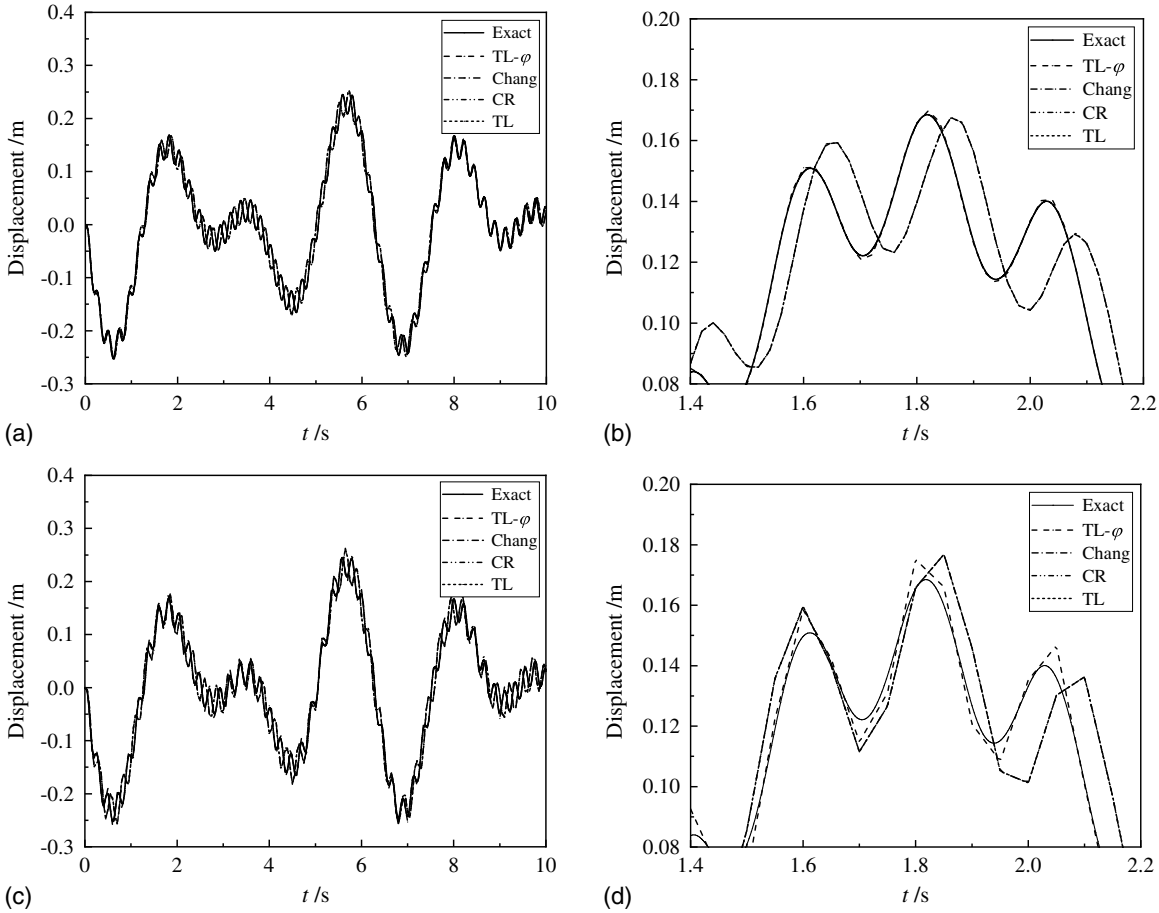

Fig. 15. Displacement responses of free vibration of a linear MDOF system: (a) $\Delta t = 0.02$ s, 0 s $\le t \le$ 10 s; (b) $\Delta t = 0.02$ s, 1.4 s $\le t \le$ 2.2 s; (c) $\Delta t = 0.05$ s, 0 s $\le t \le$ 10 s; and (d) $\Delta t = 0.05$ s, 1.4 s $\le t \le$ 2.2 s.

in the other three algorithms. When $\Delta t = 0.05$ s, the curve of TL-φ can match that of Exact well, though a small difference exists in the amplitude. The velocity and acceleration responses are shown in Figs. 16 and 17. Similar conclusions to Case 1 can be drawn that the introduction of the precorrection coefficient φ diminishes the period distortion of the responses and keep a high level of accuracy in dynamic analysis.

Case 4: Nonlinear MDOF System

A five-story shear-type frame with softening stiffness is shown in Fig. 18. The initial structural properties are $m = 10^5$ kg, $k_0 = 10^8$ N/m, and $\xi = 0.02$ before it deforms. The softening stiffness of the system after deformation is intentionally designated as $k_i = k_{i,0}(1 - 0.5\sqrt{|u_i - u_{i-1}|})$, where subscript i refers to the ith

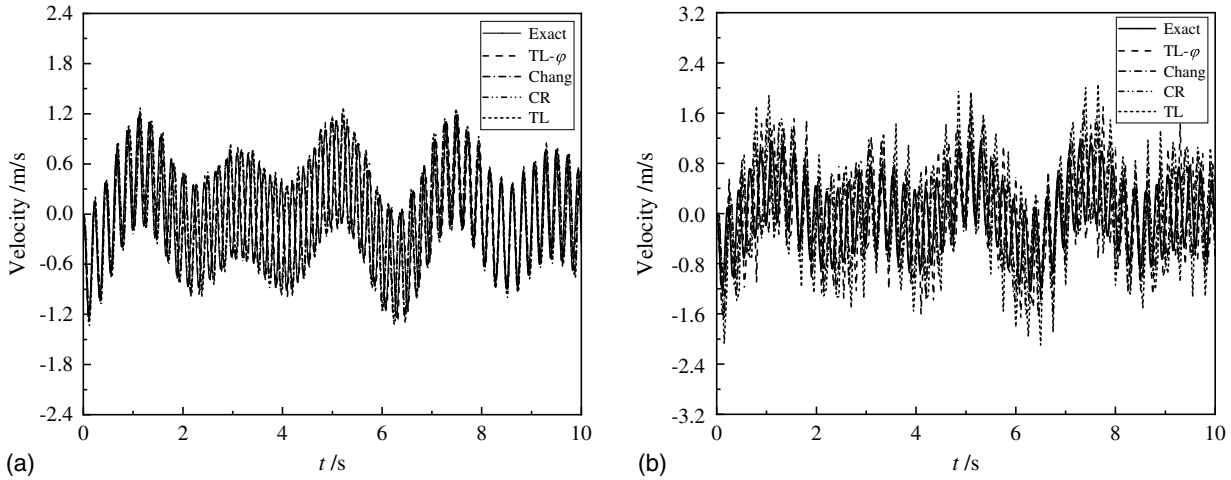

Fig. 16. Velocity responses of forced vibration of a linear MDOF system: (a) $\Delta t = 0.02$ s; and (b) $\Delta t = 0.05$ s.

J. Eng. Mech., 2021, 147(3): 04021001

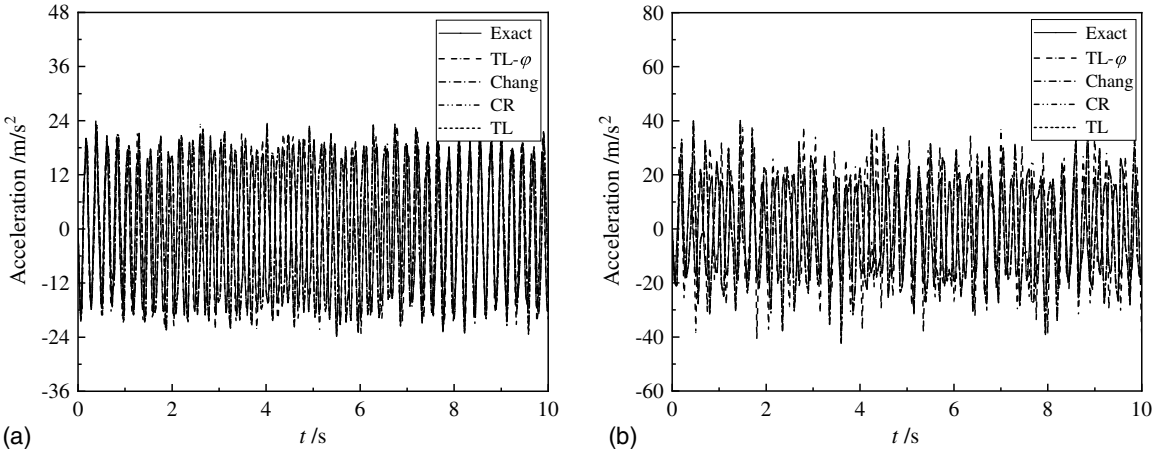

Fig. 17. Acceleration responses of forced vibration of a linear MDOF system: (a) $\Delta t = 0.02$ s; and (b) $\Delta t = 0.05$ s.

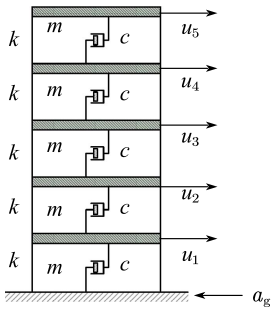

Fig. 18. Schematic diagram of a five-story shear frame building with damping.

Table 5. Displacement errors of a nonlinear MDOF system

Error index	TL-φ	Chang	CR	TL
NEE	0.9236	1.7683	1.7862	2.1386
NRMSE	2.7648	3.9656	3.9698	4.0635

story and $(u_i - u_{i-1})$ is the interstory drift for the ith story. The natural frequencies of the system are 9.0008, 26.273, 41.417, 53.206, and 60.684 rad/s for the five modes, respectively; the normalized modal matrix is given by $\boldsymbol{\Phi} = [\boldsymbol{\phi}_1 \quad \boldsymbol{\phi}_2 \quad \boldsymbol{\phi}_3 \quad \boldsymbol{\phi}_4 \quad \boldsymbol{\phi}_5]$, where $\boldsymbol{\phi}_1 = [0.2846 \quad 0.5462 \quad 0.7635 \quad 0.9190 \quad 1.0000]^T$, $\boldsymbol{\phi}_2 = [0.7635 \quad 1.0000 \quad 0.5462 \quad -0.2846 \quad -0.9190]^T$, $\boldsymbol{\phi}_3 = [1.0000 \quad 0.2846 \quad -0.9190 \quad -0.5462 \quad 0.7635]^T$, $\boldsymbol{\phi}_4 = [0.9190 \quad -0.7635 \quad -0.2846 \quad 1.0000 \quad -0.5462]^T$, and $\boldsymbol{\phi}_5 = [0.5462 \quad -0.9190 \quad 1.0000 \quad -0.7635 \quad 0.2846]^T$.

The nonlinear seismic responses of the system subjected to the ground acceleration record of El Centro (1940, NS) with peak ground acceleration (PGA) scaled to 1.03 g are obtained from the TL-φ algorithms, the Chang explicit method, the CR algorithm, and the TL algorithm with a time step of $\Delta t = 0.01$ s. In this case, $\omega_1 = 9.0008$ is taken as the critical frequency, and the corresponding φ is 0.9993. The reference solutions are calculated using the Newmark algorithm with $[\gamma, \beta] = [1/2, 1/4]$ and $\Delta t = 0.001$ s. The numerical results, including the displacement, velocity, and acceleration responses of the system for the initial conditions of $u_0 = 0$ m, $\dot{u}_0 = 0$ m/s are displayed in Table 5 and Figs. 19 and 20. Table 5 indicates that both the normalized energy errors and normalized root-mean-square errors of the TL-φ algorithms

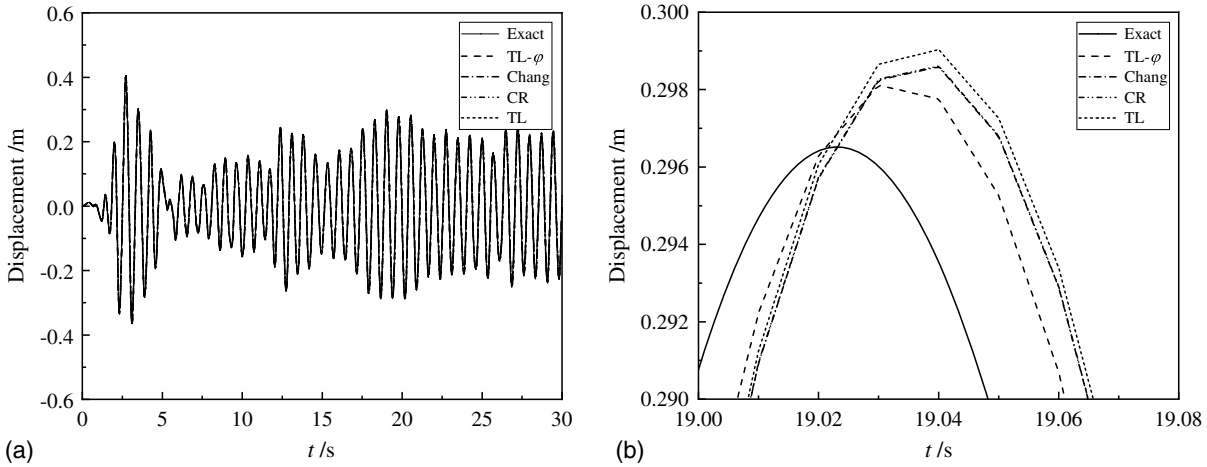

Fig. 19. Displacement responses of forced vibration of a nonlinear MDOF system: (a) 0 s $\le t \le$ 30 s; and (b) 19.00 s $\le t \le$ 19.06 s.

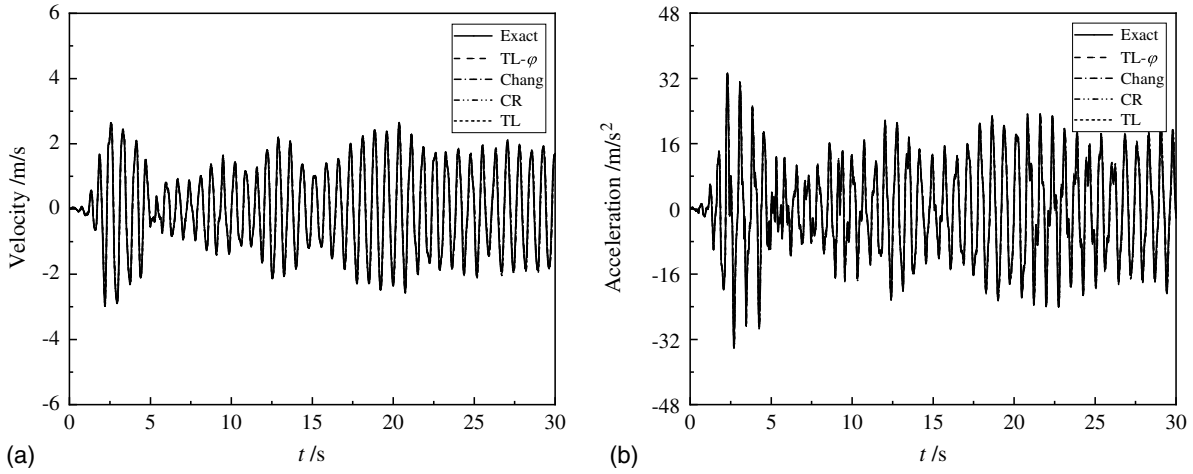

Fig. 20. Velocity and acceleration responses of forced vibration of a nonlinear MDOF system: (a) velocity; and (b) acceleration.

are smaller than the other three methods when applied in nonlinear MDOF systems. This can also be observed in Fig. 19(b), where the curve of TL-φ is closer to that of Exact than the other ones, indicating a lesser period elongation achieved by the TL-φ algorithms. Therefore, the conclusion can be drawn that the control of numerical dispersion or period distortion is achievable for nonlinear systems as well, which is a more desirable performance than the existing algorithms.

Discussion

In this paper, we present a new family of explicit integration algorithms by using a precorrection transformation from a continuous domain to a discrete domain based on the control theory, in which the displacement and velocity increments inherit from the TL algorithm. Actually, the precorrection transformation can be applied in other algorithms such as the CR algorithm, whose formulation and the corresponding integration parameters are

$$\begin{aligned} \dot{u}_{i+1} &= \dot{u}_i + \alpha_1 \Delta t \ddot{u}_i \\ u_{i+1} &= u_i + \Delta t \dot{u}_i + \alpha_2 \Delta t^2 \ddot{u}_i \end{aligned} \tag{47}$$

$$\alpha_1 = \alpha_2 = \frac{4}{4 + 4\xi\Omega + \Omega^2} \tag{48}$$

The characteristic equation of $G(z)$ derived from the precorrection transformation is

$$(\Omega^2 + 4\xi\Omega\varphi + 4\varphi^2)z^2 + (2\Omega^2 - 8\varphi^2)z + 4\varphi^2 - 4\xi\Omega\varphi + \Omega^2 = 0 \tag{49}$$

Then, the integration parameters are functions of φ and can be written as

$$\begin{aligned} \alpha_1 &= \frac{4}{\Omega^2 + 4\xi\Omega\varphi + 4\varphi^2} \\ \alpha_2 &= \frac{4 + 8\xi\varphi(1-\varphi)\Omega^{-1}}{\Omega^2 + 4\xi\Omega\varphi + 4\varphi^2} \end{aligned} \tag{50}$$

where $0 < \varphi \leq 1$ and $\varphi = \lim_{\Omega \to 0}[\arctan(\Omega/2)]/[\Omega/2] = 1$.

Here, another family of explicit integration algorithms, whose formulations inherit from the CR algorithm, are developed and referred to as CR-φ algorithms. It is noted that when $\varphi = 1$, the expressions for α_1 and α_2 are identical to those of the CR algorithm as shown in Eq. (48). Thus, the CR algorithm is a special case ($\varphi = 1$) of this family of algorithms. The stability, root locus, and stability limit for different values of φ, δ, and ξ are computed for linear and nonlinear systems, respectively, as shown in Figs. 21–23. It is observed that the CR-φ algorithms with $0 < \varphi \leq 1$ are unconditionally stable for linear and instantaneous softening stiffness systems while conditionally stable for instantaneous hardening stiffness systems. The stability limit can also be expressed as

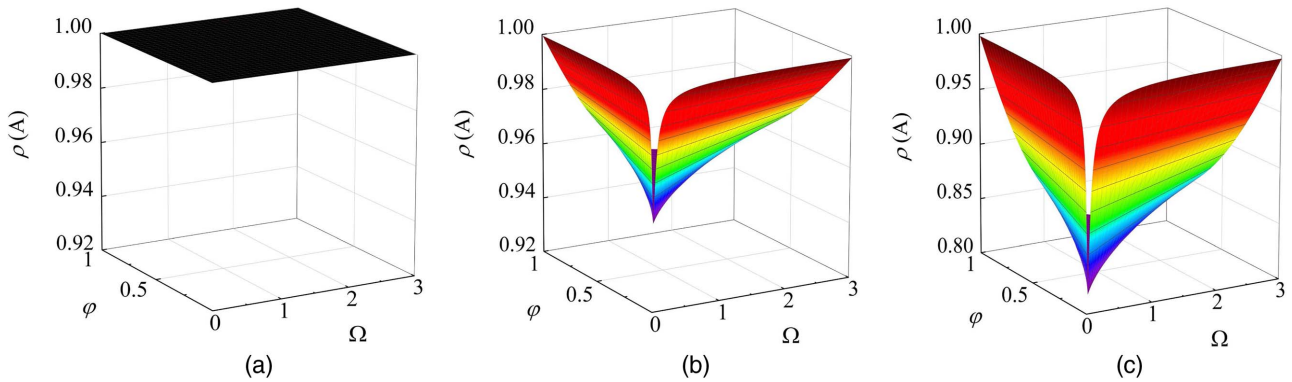

Fig. 21. Spectral radius for CR-φ algorithms for different values of ξ for linear elastic system: (a) $\xi = 0.0$; (b) $\xi = 0.05$; and (c) $\xi = 0.2$.

J. Eng. Mech., 2021, 147(3): 04021001

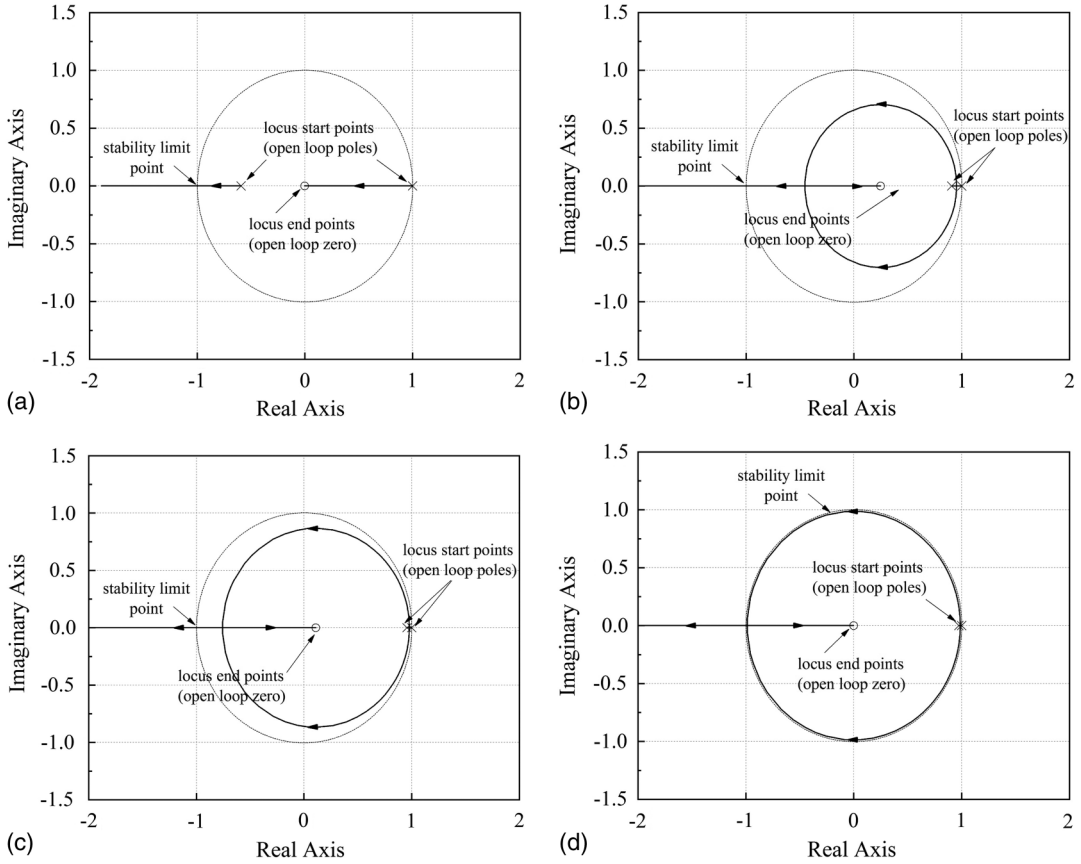

Fig. 22. Root locus of open-loop transfer function $H(z)G'(z)$ of CR-φ method with different φ: (a) $\varphi = 0.05$; (b) $\varphi = 0.5$; (c) $\varphi = 0.75$; and (d) $\varphi = 1.0$.

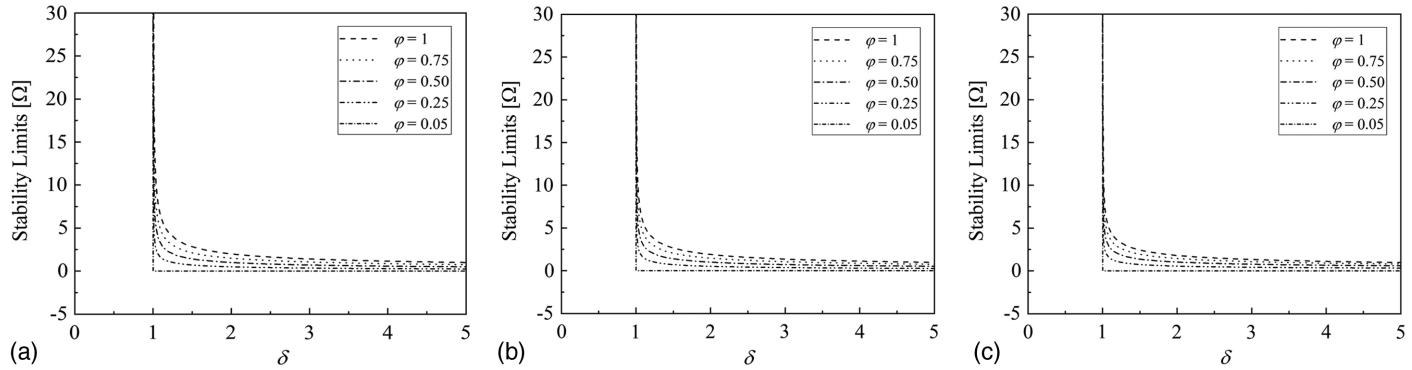

Fig. 23. Variations of upper stability limits with δ for CR-φ algorithms: (a) $\xi = 0.0$; (b) $\xi = 0.05$; and (c) $\xi = 0.20$.

$$k_{i+1} \le \frac{4m - 2\alpha_2 c\Delta t}{(2\alpha_2 - \alpha_1)\Delta t^2} \quad \text{or} \quad \frac{k_{i+1}}{k_0} \le \frac{4m - 2\alpha_1 c\Delta t}{m\Omega_0^2(2\alpha_2 - \alpha_1)} \tag{51}$$

The accuracy analysis is discussed as well. For simplicity, the relative period errors and numerical damping ratio are not displayed here as they are quite similar to those of the TL-φ algorithms, as shown in Figs. 6 and 7. It is worth noting that the introduction of precorrection parameter φ will not greatly change the main numerical characteristics, i.e., stability and numerical dissipation, of the original algorithms (such as the TL algorithm and CR algorithm) but only improve the performance of numerical dispersion.

Conclusions

A new family of explicit structure-dependent integration algorithms, named TL-φ algorithms, have been developed for structural dynamics, whose formulations inherit from the TL algorithm. By using a precorrected bilinear transformation from a continuous domain to a discrete domain associating with pole-matching based on the control theory, a precorrection parameter φ related to the critical frequency of the structure is introduced in the two integration parameters. The stability and accuracy analysis of the TL-φ algorithms present that the value of φ has a significant impact on the performance of numerical dispersion, while it will not greatly change the stability and numerical dissipation properties of the

original TL algorithm, which is verified by the discussion of applying the precorrected bilinear transformation to the CR algorithm as well.

For stability, the TL-φ algorithms are unconditionally stable for linear systems while only conditionally stable for nonlinear systems, which is the same as the TL algorithm, and the upper stability limit slightly increases with an increasing φ. For accuracy, there is no numerical dissipation for the TL-φ algorithms when applied to the zero-damping system. However, the absolute numerical damping ratio generally increases with Ω for the nonzero-damping one, and it slightly decreases with the increase of φ for a given Ω. The most desirable improvement of the proposed method is that it can diminish the relative period errors at each time step, especially the step that corresponds to the critical frequency. Meanwhile, the diminution of the relative period errors becomes more obvious for a given Ω with a smaller value of φ, so that the frequency precorrection procedure is more practical for a larger product of the critical frequency and integration step.

Four numerical examples are used to investigate the improved performance of the newly developed method. It is illustrated that a lesser period elongation can be achieved in the TL-φ algorithms when compared with other algorithms. Actually, the larger the product of the critical frequency and time step is, the smaller the normalized energy errors and normalized root-mean-square errors are, indicating a smaller period distortion. The results of all the cases show that the proposed method can be potentially used to solve linear and nonlinear structural dynamic problems with a relatively high accuracy.

Data Availability Statement

All data, models, or code generated or used during the study are available from the corresponding author by request.

Acknowledgments

This paper is based upon work supported by the National Natural Foundation of China (Grant Nos. 52008074, 41904095, and 51908048), the State Key Laboratory of Mechanical Behavior and System Safety of Traffic Engineering Structures at Shijiazhuang Tiedao University (Grant No. ZZ2020-04), and the Natural Science Foundation of Hebei Province (Grant No. E2019210350).

References

Belytschko, T., and T. Hughes. 1983. *Computational methods for transient analysis*. Amsterdam, Netherlands: Elsevier.

Bonnetr, P., M. Williams, and A. Blakeboroughg. 2008. "Evaluation of numerical time-integration schemes for real-time hybrid testing." *Earthquake Eng. Struct. Dyn.* 37 (13): 1467–1490. https://doi.org/10.1002/eqe.821.

Butcher, J. 2003. *Numerical methods for ordinary differential equations*. Chichester, UK: Wiley.

Chang, S. 1997. "Improved numerical dissipation for explicit methods in pseudodynamic tests." *Earthquake Eng. Struct. Dyn.* 26 (9): 917–929. https://doi.org/10.1002/(SICI)1096-9845(199709)26:9<917::AID-EQE685>3.0.CO;2-9.

Chang, S. 2002. "Explicit pseudodynamic algorithm with unconditional stability." *J. Eng. Mech.* 128 (9): 935–947. https://doi.org/10.1061/(ASCE)0733-9399(2002)128:9(935).

Chang, S. 2007. "Improved explicit method for structural dynamics." *J. Eng. Mech.* 133 (7): 748–760. https://doi.org/10.1061/(ASCE)0733-9399(2007)133:7(748).

Chang, S. 2009. "An explicit method with improved stability property." *Int. J. Numer. Methods Eng.* 77 (8): 1100–1120. https://doi.org/10.1002/nme.2452.

Chang, S. 2013. "An explicit structure-dependent algorithm for pseudodynamic testing." *Eng. Struct.* 46 (Jan): 511–525. https://doi.org/10.1016/j.engstruct.2012.08.009.

Chang, S. 2014. "A family of noniterative integration methods with desired numerical dissipation." *Int. J. Numer. Methods Eng.* 100 (1): 62–86. https://doi.org/10.1002/nme.4720.

Chang, S. 2016. "Improved formulation for a structure-dependent integration method." *Struct. Eng. Mech.* 60 (1): 149–162. https://doi.org/10.12989/sem.2016.60.1.149.

Chang, S. 2018. "An unusual amplitude growth property and its remedy for structure-dependent integration methods." *Comput. Methods Appl. Mech. Eng.* 330 (Mar): 498–521. https://doi.org/10.1016/j.cma.2017.11.012.

Chang, S., and W. Liao. 2005. "An unconditionally stable explicit method for structural dynamics." *J. Earthquake Eng.* 9 (3): 349–370. https://doi.org/10.1080/13632460509350546.

Chang, S., T. Wu, N. Tran, and Y. Yang. 2017. "Applications of a family of unconditionally stable, dissipative, explicit methods to pseudodynamic tests." *Exp. Tech.* 41 (1): 19–36. https://doi.org/10.1007/s40799-016-0151-4.

Chen, C., and J. Ricles. 2008a. "Development of direct integration algorithms for structural dynamics using discrete control theory." *J. Eng. Mech.* 134 (8): 676–683. https://doi.org/10.1061/(ASCE)0733-9399(2008)134:8(676).

Chen, C., and J. Ricles. 2008b. "Stability analysis of direct integration algorithm applied to nonlinear structural dynamics." *J. Eng. Mech.* 134 (9): 703–711. https://doi.org/10.1061/(ASCE)0733-9399(2008)134:9(703).

Chen, C., J. Ricles, T. Marullo, and O. Mercan. 2008. "Real-time hybrid testing using the unconditionally stable explicit CR integration algorithm." *Earthquake Eng. Struct. Dyn.* 38 (1): 23–44. https://doi.org/10.1002/eqe.838.

Chopra, A. 2001. *Dynamics of structures: Theory and applications to earthquake engineering*. 2nd ed. Upper Saddle River, NJ: Prentice-Hall.

Chung, J., and J. Lee. 1994. "A new family of explicit time integration methods for linear and non-linear structural dynamics." *Int. J. Numer. Methods Eng.* 37 (23): 3961–3976. https://doi.org/10.1002/nme.1620372303.

Clough, R., and J. Penzien. 2011. *Dynamics of structures*. 2nd ed. Beijing: Higher Education Press.

Darby, A., A. Blakeborough, and M. Williams. 2001. "Improved control algorithm for real-time substructure testing." *Earthquake Eng. Struct. Dyn.* 30 (3): 431–448. https://doi.org/10.1002/eqe.18.

Feng, Y., Z. Guo, and Y. Gao. 2018. "An unconditionally stable explicit algorithm for nonlinear structural dynamics." *J. Eng. Mech.* 144 (6): 04018034. https://doi.org/10.1061/(ASCE)EM.1943-7889.0001458.

Fu, B. 2017. "Substructure shaking table testing method using model-based integration algorithms." Ph.D. thesis, School of Civil Engineering, Tongji Univ.

Fu, B., D. Feng, and H. Jiang. 2019. "A new family of explicit model-based integration algorithms for structural dynamic analysis." *Int. J. Struct. Stab. Dyn.* 19 (6): 1950053. https://doi.org/10.1142/S0219455419500536.

Gui, Y., J. Wang, F. Jin, C. Chen, and M. Zhou. 2014. "Development of a family of explicit algorithms for structural dynamics with unconditional stability." *Nonlinear Dyn.* 77 (4): 1157–1170. https://doi.org/10.1007/s11071-014-1368-3.

Guo, J., W. Zhao, Y. Du, Y. Cao, G. Wang, and M. Zhang. 2018. "New method for real-time hybrid testing with a global iteration strategy." *J. Eng. Mech.* 144 (12): 04018218. https://doi.org/10.1061/(ASCE)ST.1943-541X.0002207.

Hilber, H., T. Hughes, and R. Taylor. 1977. "Improved numerical dissipation for time integration algorithms in structural mechanics." *Earthquake Eng. Struct. Dyn.* 5 (3): 283–292. https://doi.org/10.1002/eqe.4290050306.

Kim, W., and J. Lee. 2018. "An improved explicit time integration method for linear and nonlinear structural dynamics." *Comput. Struct.* 206 (Aug): 42–53. https://doi.org/10.1016/j.compstruc.2018.06.005.

Kolay, C., and J. Ricles. 2014. "Development of a family of unconditionally stable explicit direct integration algorithms with controllable numerical numerical energy dissipation." *Earthquake Eng. Struct. Dyn.* 43 (9): 1361–1380. https://doi.org/10.1002/eqe.2401.

Kolay, C., and J. Ricles. 2019. "Improved explicit integration algorithms for structural dynamic analysis with unconditional stability and controllable numerical dissipation." *J. Earthquake Eng.* 23 (5): 771–792. https://doi.org/10.1080/13632469.2017.1326423.

Li, J., and K. Yu. 2019. "Noniterative integration algorithms with controllable numerical dissipations for structural dynamics." *Int. J. Comput. Methods* 16 (7): 1850111. https://doi.org/10.1142/S0219876218501116.

Li, S., D. Yang, H. Guo, and G. Liang. 2020. "General formulation of eliminating unusual amplitude growth for structure-dependent integration algorithms." *Int. J. Struct. Stab. Dyn.* 20 (1): 2050006. https://doi.org/10.1142/S0219455420500066.

Newmark, N. 1959. "A method of computation for structural dynamics." *J. Eng. Mech.* 85 (3): 67–94.

Ogata, K. 2014. *Discrete-time control systems*. Beijing: Publishing House of Electronics Industry.

Rezaiee-Pajand, M., and M. Hashemian. 2016. "Time integration method based on discrete transfer function." *Int. J. Struct. Stab. Dyn.* 16 (5): 1550009. https://doi.org/10.1142/S0219455415500091.

Rustemovic, M., and T. Uzunovic. 2018. "Comparison of different methods for digital fractional-order differentiator and integrator design." In *Proc., 41st Int. Conf. on Telecommunications and Signal Processing*, 350–355. New York: IEEE.

Shing, P. B., and S. A. Mahin. 1985. "Computational aspects of a seismic performance test method using on-line computer control." *Earthquake Eng. Struct. Dyn.* 13 (4): 507–526. https://doi.org/10.1002/eqe.4290130406.

Tang, Y., and M. Lou. 2017. "New unconditionally stable explicit integration algorithm for real-time hybrid testing." *J. Eng. Mech.* 143 (7): 04017029. https://doi.org/10.1061/(ASCE)EM.1943-7889.0001235.

Tang, Y., and M. Lou. 2018. "Closure to 'New unconditionally stable explicit integration algorithm for real-time hybrid testing' by Yu Tang and Menglin Lou." *J. Eng. Mech.* 144 (10): 07018004. https://doi.org/10.1061/(ASCE)EM.1943-7889.0001522.

Wang, C., X. Liu, and Y. Ji. 2008. *Continuous and discrete control system*. Beijing: Science Press.

Wang, T., H. Zhou, X. Zhang, and T. Ran. 2018. "Stability of an explicit time-integration algorithm for hybrid tests, considering stiffness hardening behavior." *Earthquake Eng. Struct. Vibr.* 17 (3): 595–606. https://doi.org/10.1007/s11803-018-0465-6.

Wilson, E., I. Farhoomand, and K. Bathe. 1973. "Nonlinear dynamic analysis of complex structure." *Earthquake Eng. Struct. Dyn.* 1 (3): 241–252. https://doi.org/10.1002/eqe.4290010305.

Xia, C. 2018. *Modern control theory.* Beijing: Science Press.

Yu, K., and J. Zou. 2016. *Dynamics of structure*. Harbin, China: Harbin Institute of Technology Press.

Zhai, W. 1996. "Two simple fast integration methods for large-scale dynamic problems in engineering." *Int. J. Numer. Methods Eng.* 39 (24): 4199–4214. https://doi.org/10.1002/(SICI)1097-0207(19961230)39:24<4199::AID-NME39>3.0.CO;2-Y.